

# ABUNDANCE PATTERNS IN THE DRACO, SEXTANS AND URSA MINOR DWARF SPHEROIDAL GALAXIES

MATTHEW D. SHETRONE

McDonald Observatory, University of Texas, P.O. Box 1337, Fort Davis, Texas 79734  
 shetrone@astro.as.utexas.edu

PATRICK CÔTÉ<sup>1</sup>

California Institute of Technology, Mail Stop 105-24, Pasadena, CA 91125, and  
 Department of Physics & Astronomy, Rutgers University, 136 Frelinghuysen Road, Piscataway, NJ  
 08854-8019

pcote@physics.rutgers.edu

AND

W.L.W. SARGENT

California Institute of Technology, Mail Stop 105-24, Pasadena, CA 91125  
 wws@astro.caltech.edu

*Accepted for publication in the Astrophysical Journal*

## ABSTRACT

The Keck I telescope and the High Resolution Echelle Spectrometer (HIRES) have been used to obtain spectra for red giant stars belonging to the Draco, Sextans and Ursa Minor dwarf spheroidal (dSph) galaxies. An analysis of these spectra is presented, along with abundance ratios for more than 20 elements. The resulting database of element abundances for 17 dSph stars is the most extensive yet assembled for stars in such environments. Our principal findings are summarized as follows: (1) There is unambiguous evidence for a large internal dispersion in metallicity in all three galaxies: our program stars span a range of  $\Delta[\text{Fe}/\text{H}] = 1.53, 1.40$  and  $0.73$  dex in Draco, Sextans and Ursa Minor, respectively. (2) The abundance patterns among the dSph stars are remarkably uniform, suggesting that three galaxies have similar nucleosynthetic histories and, presumably, similar initial mass functions. (3) A comparison of the measured element abundance ratios for our sample of dSph stars with published values for Galactic halo and disk field stars suggests that the dSph galaxies have  $0.02 \lesssim [\alpha/\text{Fe}] \lesssim 0.13$  dex, whereas the halo field star sample has  $[\alpha/\text{Fe}] \sim 0.28$  dex over the same range in metallicity. (4) The most metal-rich dSph stars in our sample have  $[\text{Y}/\text{Fe}]$  abundances which are significantly lower than those measured for halo field stars of similar metallicity, while the measured  $[\text{Ba}/\text{Eu}]$  ratios for the dSph stars suggest that the early chemical evolution of these galaxies was dominated by the r-process. Taken together, these results suggest that the Galactic halo is unlikely to have assembled, *in its entirety*, through the disruption of dwarf galaxies similar to the low-luminosity,  $\langle L_V \rangle = 3 \times 10^5 L_{V,\odot}$ , dSphs studied here. We also note that the measured  $[\text{Zn}/\text{Fe}]$  abundance ratios for the dSph stars exceed those of damped Ly $\alpha$  systems having low levels of dust depletion by roughly an order of magnitude.

The first high-resolution abundance analysis for the distant Galactic globular cluster NGC 2419 is also presented. From a HIRES spectrum of a single red giant, we find a metallicity of  $[\text{Fe}/\text{H}] = -2.32 \pm 0.11$  dex. This is slightly lower than, but still consistent with, published estimates based on low-resolution spectroscopy. With the possible exception of a slight enhancement in the abundances of some heavy elements such as Ce, Nd, Y and Ba, the observed abundance pattern closely resembles those exhibited by red giants in M92: a nearby, well-studied globular cluster of nearly identical metallicity.

*Subject headings:* stars: abundances — galaxies: abundances — galaxies: dwarf — galaxies: individual (Draco, Sextans, Ursa Minor) — quasars: absorption lines

## 1. INTRODUCTION

As isolated, low-mass systems, dwarf galaxies are probably the closest approximations in Nature to idealized “closed” or “leaky box” models of chemical enrichment. The old, nearby dwarf satellites of the Milky Way thus offer a unique opportunity to study the formation and chemical evolution of galaxies in a level of detail which will never be possible with high-redshift systems.

The apparent dearth of gas and young stars in the Galactic dwarf spheroidal (dSph) galaxies, coupled with their low metallicities, led early researchers to regard them

as similar to globular clusters in terms of their stellar populations (*e.g.*, Hodge 1971), despite clear differences in their respective structural parameters. However, careful scrutiny has now revealed these systems to be far from simple. Mateo (1998) recently reviewed the now overwhelming observational evidence for complex and varied star formation histories in these faint systems. High-precision photometric studies, and low-resolution spectroscopy of individual red giant branch (RGB) stars, has firmly established that both Galactic and M31 dSph galaxies show evidence for large internal metallicity variations (*e.g.*, Zinn 1978; Stetson 1984; Suntzeff et al. 1993; Côté, Oke &

<sup>1</sup>Sherman M. Fairchild Fellow

Cohen 1999; Da Costa et al. 2000). Recently, Shetrone, Bolte & Stetson (1998; hereafter SBS) presented an abundance analysis for four RGB stars belonging to the Draco dSph galaxy: the first study of dSph stars to make use of high-resolution ( $R = 34,000$ ) spectroscopy. SBS measured abundance ratios for a variety of elements and, despite the limited sample size, found unmistakable evidence for a wide range in metallicity of  $-3 \lesssim [\text{Fe}/\text{H}] \lesssim -1.5$  dex.

Elemental abundances represent a potentially powerful means of testing the suggestion that dwarf galaxies are the surviving “building blocks” from which larger galaxies formed (Larson 1988; Zinn 1993). Such tests are particularly topical in view of the emerging empirical and analytical evidence that galactic halos are assembled from chemically-distinct, low-mass fragments (*e.g.*, Searle & Zinn 1978; Zinn 1993; Ibata et al. 1994; Klypin et al. 1999; Moore et al. 1999; Côté et al. 2000; Yanny et al. 2000). Some hydrodynamical simulations of galaxy formation also point to the assembly of large galaxies from low-mass, gas-rich, proto-galactic fragments (*i.e.*, Haehnelt, Steinmetz & Rauch 1998; 2000). If these gaseous fragments are the high-redshift analogs of local dwarf galaxies, then a correspondence between the abundance patterns of the dSphs and those of damped Ly $\alpha$  (DLA) absorbers might be expected; such a correspondence in the *mean* metallicities has been known for some time (see Pettini et al. 1997 and references therein), although the association of DLA systems with spiral disks (Wolfe et al. 1995; Prochaska & Wolfe 1997) or dwarf galaxies (York et al. 1986; Tyson 1988; Pettini, Boksenberg & Hunstead 1990) remains an open question. By examining the abundance patterns of dSph galaxies, and comparing with those of DLA systems and Galactic halo/disk field stars, it may be possible to discriminate between these different scenarios.

In this paper, we build upon the initial study of SBS by analyzing high-resolution spectra for an expanded sample of RGB stars belonging to the Draco, Sextans and Ursa Minor dSph galaxies, as well as for a single red giant in the distant globular cluster NGC 2419. We compare the element abundance ratios measured for our sample of dSph stars to those of Galactic halo/disk field stars and DLA absorbers having low levels of dust depletion.

## 2. OBSERVATIONS AND REDUCTIONS

### 2.1. Selection of Program Stars

RGB stars belonging to three Galactic dSph galaxies (*i.e.*, Draco, Sextans and Ursa Minor) were selected from a combination of published color-magnitude diagrams, new unpublished magnitudes (Stetson 2000, private communication and Cudworth 2000, private communication) and radial velocity catalogs (*e.g.*, Da Costa et al. 1991; Suntzeff et al. 1993; Stetson 1979, 1984; Armandroff, Olaszewski & Pryor 1995). Published radial velocities were used to ensure that only *bona fide* members of their respective galaxies were targeted for observation with HIRES, the High Resolution Echelle Spectrometer on the Keck I 10m telescope (Vogt et al. 1994).

Color magnitude diagrams for the three dSph galaxies studied here are shown in Figure 1. RGB stars for which we have HIRES spectra are indicated by the large sym-

bols. These three galaxies contain little or no gas (Blitz & Robishaw 2000) and are comprised predominantly of old stars, although Mateo, Fischer & Krzemiński (1995 report the presence of a modest intermediate-age population in Sextans. The four Draco red giants observed by SBS are also shown in Figure 1, as we have re-analyzed their spectra here (see §4). The lower right panel of Figure 1 shows the distribution of our sample of RGB stars in the  $M_V$ -( $B-V$ )<sub>0</sub> plane. The dashed lines in this panel show 13 Gyr isochrones from Bergbusch & Vandenberg (1992) having metallicities of  $[\text{Fe}/\text{H}] = -2.26, -1.66$  and  $-1.26$  dex.

### 2.2. HIRES Spectroscopy

HIRES spectra for 13 RGB stars belonging to the Draco, Ursa Minor and Sextans dSph galaxies were acquired during three observing runs at the Keck I telescope. During the March 1999 observing run, we also obtained a spectrum of a single red giant in the outer-halo globular cluster NGC 2419. A number of bright RGB stars belonging to the nearby, well-studied globular clusters M92 and M3 were also observed during the March 1999 and July 1999 observing runs, in order to compare our measured abundances with those of previous high-resolution spectroscopic studies. An observing log for these observations is presented in Table 1. For each run, we used the C5 decker to produce a  $1''.15 \times 7''$  slit and a spectral resolution of  $\lambda/\Delta\lambda = 34,000$ . In all cases, the detector was binned  $1 \times 2$  in the spatial direction in order to reduce the read noise. Spectra obtained during the July 1999 and August 1999 observing runs span the wavelength region  $4540 \lesssim \lambda \lesssim 7020$  Å; different echelle and cross disperser angles were used during the March 1999 observations, giving a wavelength coverage of  $3850 \lesssim \lambda \lesssim 6300$  Å. The raw spectra were reduced using the MAKEE software package (Tom Barlow, private communication), and wavelength-calibrated within the IRAF<sup>2</sup> environment.

Table 2 summarizes several properties of the program stars. From left to right, this table records the star name,  $V$  magnitude, ( $B-V$ ) color, interstellar extinction, HIRES exposure time, signal-to-noise ratio (S/N) measured at the continuum near  $\lambda \simeq 6100$  Å, and heliocentric Julian date. The final column records the heliocentric radial velocity of each star, measured directly from the spectra with the velocity zero-point established using telluric lines (see Shetrone 1994). References for the photometry are given in the notes to the table. For all objects, the adopted reddening is taken from the DIRBE reddening maps of Schlegel, Finkbeiner & Davis (1998).

## 3. ANALYSIS

The lines chosen for the abundance analysis were adopted from several sources, including Blackwell et al. (1982), Blackwell et al. (1986), Bizzarri et al. (1993), Fuhrmann et al. (1995), McWilliam et al. (1995; M95), Kraft et al. (1995), Shetrone (1996), Sneden et al. (1996), Carretta & Gratton (1997), and the National Institute of Standards and Technology Atomic Spectra Database. In some cases, the line choices differ from those of SBS, mainly in the addition of more and better lines for Ti I, Ti II, Mg I and several rare earth elements. Equivalent

<sup>2</sup>IRAF is distributed by the National Optical Astronomy Observatories, which are operated by the Association of Universities for Research in Astronomy, Inc., under contract to the National Science Foundation.

widths (EWs) were measured from Gaussian fits to individual spectra lines. Table 3 lists the measured EWs and adopted line parameters for each of the elements considered below.

Figure 2 shows a comparison of our EWs for the M92 and M3 RGB stars which we have in common with Sneden et al. (1991) and Kraft et al. (1992). There is an essentially no offset,  $\Delta\text{EW} = 1.6 \pm 1.2 \text{ m\AA}$ , between the two datasets, and the rms scatter of  $\sigma = 7.1 \text{ m\AA}$  is consistent with the errors expected from uncertainties of the individual measurements. These results are consistent with those found in SBS.

Initial temperature estimates were made using the colors and reddenings from Table 2, using the de-reddened colors,  $(B - V)_0$ , and our own  $(B - V)_0$ - $T_{\text{eff}}$  calibration for red giants with metallicities in the range  $-3.0 \leq [\text{Fe}/\text{H}] \leq -1.0$  dex. These initial estimates were based on rough approximations of the metallicities of the program stars based upon their location in the color magnitude diagrams. This estimate was then fine-tuned in two ways. First, the metallicity from the first iteration was fed back into our color temperature estimate and the entire process was repeated until we converged upon a best color temperature. Second, we adjusted the color temperature by: (1) demanding a minimized slope, to within the errors, in the plots of Fe abundance (from Fe I) versus both excitation potential and equivalent width and; (2) requiring that the abundance of the *ionized* species equal that of the *neutral* species (based largely upon Fe I and Fe II, and to a lesser extent, Ti I and Ti II). In making this minimization, the microturbulent velocity, effective temperature and surface gravity were adjusted iteratively.

Among the sample of reference stars in M92 and M3, the largest deviation between the initial and final adopted parameters were  $\Delta T_{\text{eff}} = 75 \text{ K}$  and  $\Delta \log g = 0.10$  dex for the effective temperature and surface gravity, respectively. Even in the case of the much lower S/N spectrum of the red giant RH-10 in NGC 2419, the deviations were only  $-25 \text{ K}$  and  $0.1$  dex. For the sample of dSph stars, the largest deviation from the predicted temperature was  $175 \text{ K}$  for Ursa Minor K. This giant has obvious  $\text{C}_2$  bands which reveal it to be a carbon star; it is not surprising that the color temperature based upon non-carbon stars would predict a significantly cooler temperature than the actual spectroscopic effective temperature. Excluding this star, the average differences between the predicted and adopted temperatures were  $+63 \pm 18$ ,  $+38 \pm 25$  and  $+22 \pm 18 \text{ K}$  in Ursa Minor, Draco and Sextans, respectively. The differences in the predicted versus adopted surface gravities are  $-0.1 \pm 0.1$ ,  $0.0 \pm 0.2$  and  $-0.15 \pm 0.1$  dex. These slight differences in the stellar parameters could arise in several ways: a slight underestimation ( $0.02 \text{ mag}$ ) of the true reddenings, the use of a halo star  $(B - V)_0$ - $T_{\text{eff}}$  relation for the dSph giants (see §5.1), systematic errors in the unpublished photometry, or a systematic error due to working with low-S/N spectra. We reject this last possibility because the predicted and adopted parameters for NGC 2419 RH-10, which has a lower S/N ratio than the majority of the dSph spectra, are in excellent agreement, while the dSph giants having the highest S/N spectra (*i.e.*, those in Ursa Minor) exhibit the largest deviations.

Model atmospheres were taken from the computations

of the MARCS code (Gustafsson et al. 1975), and the abundance calculations were performed using the current version of Sneden's (1973) LTE line analysis and spectrum synthesis code. The procedures are nearly identical to those employed in SBS, except for the modified line list. Since some important lines were added, we have re-analyzed the Draco giants from SBS and included the results in this paper. It is important to note that, as with most high-resolution spectroscopic analyses of metal-poor stars using the MARCS models, we have compensated for the increased electron contribution from the overabundant alpha elements by slightly increasing the overall metallicity ( $+0.1$  dex) of the model atmospheres. This compensation for alpha element enhancement will be discussed further in §5.1. The best-fit model parameters for each star, along with the measured EWs, are recorded in Table 3.

Note that several of the elements in our analysis (*e.g.*, V, Mn, Ba, Eu) are known to exhibit hyper-fine splitting. We have not included this hyper-fine splitting in our analysis because our goal is the measurement of overall abundance *differences*, not absolute abundances. The magnitude of the correction is small in comparison to the EW measurement errors: *i.e.*, for  $[\text{Ba}/\text{Fe}]$  the effect is only  $0.02$  dex.

#### 4. ABUNDANCES

The first important result of this work is the overall abundance spread within the three dSph galaxies. In Figure 1, the alpha-enhanced isochrones of Bergbusch & Vandenberg (1992) are overlaid on the color-magnitude diagrams, with our sample of dSph stars indicated. If the galaxies are comprised primarily of old and coeval stars, and if the photometric uncertainties are negligible, then a metallicity range of  $-2.5 \lesssim [\text{Fe}/\text{H}] \lesssim -1.5$  dex can be expected in all three galaxies. As Table 4 shows, our measured abundances are roughly consistent with this expectation: *i.e.*, we find metallicity ranges of  $\Delta[\text{Fe}/\text{H}] \simeq 1.53$ ,  $1.40$  and  $0.73$  dex, respectively, for Draco, Sextans and Ursa Minor. Moreover, the stars with the lowest abundances are found close to the blue edge of the color distribution, as expected. A more detailed isochrone-age analysis is beyond the scope of this paper since, as discussed in §5.1, the current set of alpha-enhanced isochrones may not be entirely appropriate for these galaxies.

The weighted mean metallicities of the three dSph samples are  $\langle [\text{Fe}/\text{H}] \rangle = -2.00 \pm 0.21$ ,  $-1.90 \pm 0.11$  and  $-2.07 \pm 0.21$  dex for Draco, Ursa Minor and Sextans, respectively. Despite the small sample sizes, and the presence of large internal metallicity spreads within all three galaxies, these mean values are in good agreement with previous determinations (see, *e.g.*, Mateo 1998). The mean metallicity of the lone red giant in NGC 2419 is found to be  $[\text{Fe}/\text{H}] = -2.32 \pm 0.11$  dex. This is slightly lower than, but still consistent with, the value of  $[\text{Fe}/\text{H}] = -2.10 \pm 0.15$  dex found by Suntzeff, Kraft & Kinman (1988) from low-resolution spectroscopy of six red giants.

##### 4.1. Light Elements

Many of the light elements such as O, Na, Mg, Al are known to exhibit significant star-to-star variations in globular clusters. For instance, Shetrone (1996), Kraft et al. (1997) and Sneden et al. (1997) find large ranges in the abundances of these light elements for red giants belonging to M3 and M92:  $-0.7 < [\text{O}/\text{Fe}] < +0.45$  dex;  $-0.3 <$

$[\text{Na}/\text{Fe}] < +0.5$  dex;  $-0.1 < [\text{Mg}/\text{Fe}] < +0.4$  dex; and  $0.0 > [\text{Al}/\text{Fe}] > +1.1$ . By contrast, halo field stars do not exhibit these abundance variations. The observed variations in the globular cluster stars follow a specific pattern which is sometimes referred to as a “deep mixing abundance pattern”, with Al and Na being enhanced, and O (and sometimes Mg) being depleted. Any comparison of the dSph abundance patterns for these elements with those of the globular cluster stars is complicated by these variations. In Figure 3, the light element abundances for our program stars are shown along with a sample of Milky Way halo and disk stars. At least three of the M92 giants and one of the M3 giants exhibit the aforementioned “deep mixing abundance pattern”. Unfortunately, most of the O, Na and Al abundances for the dSph stars are upper limits, making a detailed comparison with the field star sample impossible.

#### 4.2. Even-Z ( $\alpha$ ) Elements

The light elements with even numbers of protons (*e.g.*, O, Mg, Si, Ca, Ti) are sometimes referred to as  $\alpha$  elements, or even-Z elements. Figure 4 shows our measured abundances for these even-Z elements, except for O and Mg which are shown in Figure 3, plotted against the iron abundance. The abundances of the globular cluster stars — M3, M92 and NGC 2419 — are consistent with those of the halo field stars. The Galactic halo field stars exhibit  $\alpha$ -enhancements between 0.1 and 0.5 dex (with the exception of [Si/Fe] which shows a much broader distribution) over the metallicity range  $-3.0 \lesssim [\text{Fe}/\text{H}] \lesssim -1.2$  dex. Due to the large intrinsic spread among the Si abundances, and because of our rather large errors and upper limits on the measured Si abundances, the [Si/Fe] abundance pattern will be discussed no further. The bottom panel in Figure 4 gives *average* even-Z abundances,  $[\alpha/\text{Fe}] = \frac{1}{3}([\text{Mg}/\text{Fe}] + [\text{Ca}/\text{Fe}] + [\text{Ti}/\text{Fe}])$ , for both our program stars and for those stars taken from the literature. This definition excludes the contribution from [O/Fe] since many of the stars (both in our sample and in the literature) do not have detected O lines.

A first impression from Figure 4 is that the stars belonging to the three different dSph galaxies occupy the same portion of the figures: *i.e.*, they have roughly the same abundance patterns. In addition, their abundance pattern appears to differ from that of the Galactic halo field star sample, with the dSph stars falling below the Milky Way sample at a given metallicity. Considering the dSph samples separately, the average even-Z abundances,  $[\alpha/\text{Fe}]$ , are:  $0.09 \pm 0.02$  dex for Draco,  $0.13 \pm 0.04$  dex for Ursa Minor, and  $0.02 \pm 0.07$  dex for Sextans. Over the same range in metallicity, the halo field star sample has a mean value of  $[\alpha/\text{Fe}] = 0.28 \pm 0.02$  dex. Thus, all three dSph samples have a statistically significant underabundance of Mg, Ca and Ti in comparison to the Galactic halo. By contrast, we find  $[\alpha/\text{Fe}] \simeq 0.21 \pm 0.10$  dex for the lone red giant in NGC 2419, which is slightly lower than, but nevertheless consistent with, the mean value of  $0.34 \pm 0.04$  dex for the red giants in M92.

There is also some evidence for a trend of decreasing  $[\alpha/\text{Fe}]$  abundance with increasing metallicity in the Sextans and Ursa Minor samples. The Ursa Minor sample is linearly correlated with a slope of  $d[\alpha/\text{Fe}]/d[\text{Fe}/\text{H}] = -0.26 \pm 0.11$ . The trend is less obvious among sample of

Sextans stars, which have a slope of  $-0.12 \pm 0.08$ . Nonetheless, it is certainly true that the most metal-rich star in the Sextans sample has a significantly lower even-Z abundance than the rest of the Sextans sample. Similarly, the most metal-rich star in the Draco sample has the lowest [O/Fe] and [Mg/Fe] abundance ratios for this galaxy.

#### 4.3. Iron Peak Elements

Figures 5 and 6 show the iron peak element abundance ratios plotted against metallicity. The [V/Fe] abundances are under-sampled due to the temperature sensitive nature of these lines: *i.e.*, the more metal-poor stars are hotter and hence the V lines are weaker due to both the lower abundances and the cooler temperatures. All of the dSph giants with measured V abundances exhibit the same abundance pattern as that of the halo field star sample, with the exception of Draco 473. This may be a further indication of chemical peculiarity of this metal-rich star, or it could indicate a problem with our adopted temperature.

Among the halo field stars more metal rich than  $[\text{Fe}/\text{H}] \simeq -1.9$  dex, Co and Cr are found in their solar ratios; at lower metallicities, the abundances of Co and Cr diverge, with the [Co/Fe] ratios increasing and the [Cr/Fe] ratios decreasing. This same abundance pattern is seen in each of the three dSph samples. Like [Cr/Fe], the [Cu/Fe] and [Mn/Fe] abundances exhibit a decline with decreasing iron abundance, although the onset occurs at higher metallicity. All three dSph samples exhibit sub-solar [Cu/Fe] and [Mn/Fe] abundance ratios, consistent with that found in the Milky Way sample. In addition, both [Ni/Fe] and [Zn/Fe] are found in their solar ratios in the halo and dSph samples over the metallicity range of interest.

For NGC 2419, the measured [Cr/Fe], [Mn/Fe], [Co/Fe], [Ni/Fe] and [Cu/Fe] abundances are similar to those found for the red giants in M92.

#### 4.4. Heavy Metals

We define the heavy metals as those elements with  $Z > 30$ . This broad definition includes many subcategories including the first s-process elements, the second s-process elements, and the r-process elements. The s-process elements are those produced mainly by slow neutron addition, while the r-process elements are created largely through the rapid addition of neutrons. Table 4 of Burris et al. (2000) gives the relative contributions of the s- and r-processes for all of the heavy elements in the sun. Of the heavy metals for which we have measured abundances, we have one first s-process peak element (Y), three second s-process peak elements (Ba, Ce, Sm), one r-process element (Eu) and one element which is nearly an even mix of the s- and r-processes (Nd). Figures 7 and 8 show the heavy metal abundances for the dSph, halo and globular cluster samples.

While the concept of s-process elements and r-process elements is a traditional one, it can lead to possible misconceptions. In most Population II stars, the r-process dominates and the s-process contributes little to the abundance of the “second s-process peak elements”. A notable exception to this trend is found among carbon stars. These asymptotic giant branch (AGB) stars have contaminated atmospheres, with anomalously high fractions of carbon and s-process elements on their surfaces. As a result, their

spectra are rich in  $C_2$  bands and the lines of s-process elements. One star in our sample, Ursa Minor K, has a spectrum with strong  $C_2$  bands, as noted previously from lower resolution spectroscopy (Canterna & Schommer 1978, Aaronson et al. 1983, Armandroff, Olszewski & Pryor 1995). Our analysis reveals an abundance pattern for this star which is dominated by the s-process, and confirms the classification of Ursa Minor K as a carbon star.

The abundance ratio  $[Ba/Eu]$  is most often used to access the relative contribution of the r- and s-processes to the heavy metal abundance pattern. Figure 8 shows the measured  $[Ba/Eu]$  ratios plotted against metallicity for our program stars. For the halo field star sample, the  $[Ba/Eu]$  abundances range from solar-like ratios in the most metal-rich stars, to  $[Ba/Eu] \simeq -0.5$  for  $[Fe/H] \lesssim -1$  dex. This trend can be understood as a evolution from old metal-poor stars having abundance patterns dominated by the r-process, to younger solar-metallicity stars with a mix of r-process and s-process patterns. Unfortunately, the spectrograph setup used during the observation of stars in Sextans did not include the lone Eu line which was included in the Draco and Ursa Minor spectra. For this reason, we do not have a  $[Ba/Eu]$  ratio for the Sextans stars, and hence no information about the relative r- and s-process contributions. However, the Draco and Ursa Minor stars (Ursa Minor K excluded) exhibit the same r-process dominated abundance pattern as does the Milky Way sample.

Inspection of Table 4 and Figures 7 and 8 reveals three stars whose heavy element abundance ratios are enhanced relative to those typical for other dSph and halo field stars: Ursa Minor K, Ursa Minor 199 and Sextans 35. As mentioned above, Ursa Minor K is an obvious carbon star with an enhanced s-process dominated abundance pattern, while the heavy element abundance pattern for Ursa Minor 199 is dominated by the r-process. Unfortunately, we do not know what process dominates the heavy element abundance pattern for Sextans 35, since we lack a measured Eu abundance for this star. The enhancement of the heavy element abundances for these stars does have a precedent among halo field stars; a small percentage of Population II stars which show r-process dominated heavy element abundance patterns have large over abundances of the heavy elements with respect to iron (*e.g.*, Westin et al. 2000, Norris et al. 1997, Cowan et al. 1995).

Excluding the three dSph stars with large overabundances of the heavy elements, the abundances of the second s-process elements (Ce, Sm, and Ba) are consistent with those of the halo field stars. This is also true for the abundances of the r-process peak element Eu. However, the abundances of Y (a first s-process peak element) are much lower in the more metal-rich dSph giants than in the halo field stars of similar metallicity. In the bottom panel of Figure 8, we have plotted the  $[Ba/Y]$  abundance ratio against the metallicity. It is clear that the dSph sample has a significantly higher  $[Ba/Y]$  abundance ratio than the halo field star sample over the entire range of dSph metallicities.

For NGC 2419, the measured ratios of  $[Ce/Fe]$ ,  $[Nd/Fe]$ ,  $[Y/Fe]$  and  $[Ba/Fe]$  appear to be slightly enhanced over their respective ratios in the M92 giants. Interestingly, the inferred ratio of  $[Ba/Y] = -0.13 \pm 0.14$  is in good agreement with the corresponding values measured for red

giants in M92.

## 5. DISCUSSION

The abundance patterns of the three dSphs sampled here are remarkably uniform. This suggests that the galaxies share fairly similar nucleosynthetic histories, and thus, similar initial mass functions. Because dwarf galaxies (and DLA systems) have been invoked in numerous models for the formation of large galaxies, we now address the issue of how Sextans, Draco and Ursa Minor as a group fit into these scenarios.

### 5.1. Milky Way Comparison

As mentioned above, there are some significant differences between the abundance patterns in the Milky Way and the dSph samples. Probably the most important of these is the lower even-Z abundances found among the dSph stars. Since the production of even-Z elements is thought to be dominated by massive Type II supernovae (*e.g.*, Tsujimoto, et al. 1995), lower  $[\alpha/Fe]$  abundance ratios would require either that the most massive Type II supernovae were absent in the young dSphs, or that the ejecta from these massive supernovae were lost from the galaxy and not incorporated in the subsequent generations of stars. Alternatively, it is possible that the chemical evolution of the dSph galaxies included a relatively large contribution from Type Ia supernovae (which are expected to produce large quantities of iron peak elements compared to the  $\alpha$ -elements).

The importance of the low  $[\alpha/Fe]$  abundance ratios should not be understated. The even-Z elements are abundant electron donors and hence important sources of atmospheric opacity in K giants; thus, the abundances of even-Z elements influence age estimates based upon isochrone fitting (*e.g.*, Bergbusch & Vandenberg 1992). As mentioned in §3, the analysis of halo stars includes the extra electron contribution to the opacities due to the even-Z elements, which is offset by artificially inflating the metallicity of the model atmosphere. We have followed this same procedure for the dSph stars; if this compensation were not included, the abundances of the neutral species would *increase* by 0.03 dex, while the abundance of the ionized species would *decrease* by 0.03 dex. Since our metallicities are based mainly upon the large number of Fe I lines, we may have underestimated the dSph abundances systematically by 0.03 dex. The abundance ratios for the neutral species should not change, but the abundance ratios reported in Table 4 for the ionized species may be systematically too large by 0.06 dex for stars which do not have enhanced abundances of even-Z elements.

Although the Galactic halo does contain stars with low even-Z abundance patterns (*e.g.*, Ivans et al. 2000), such stars are rare. The observed differences in the respective even-Z element abundance patterns may therefore put some interesting limitations on the suggestion that the Milky way was assembled from “building blocks”, or proto-Galactic fragments, similar to the dSphs sampled here (*e.g.*, Searle & Zinn 1978; Larson 1988; Zinn 1993; Mateo 1996; Côté et al. 2000). If these suggestions are correct, then perhaps the actual proto-Galactic fragments were larger and could better retain gas from massive Type II supernovae than the present sample of low-luminosity dSph galaxies. In the Monte-Carlo simulations of Côté et

al. (2000), the initial population of proto-Galactic fragments span a wide range in luminosities, including a small number of large systems with present-day luminosities of  $L_V \sim 2 \times 10^8 L_{V,\odot}$  as well as numerous small objects with luminosities similar to those of Draco, Sextans and Ursa Minor:  $\langle L_V \rangle \sim 3 \times 10^5 L_{V,\odot}$ . If the chemical enrichment of the proto-Galactic fragments can be roughly approximated by a Closed Box model (*e.g.*, Talbot & Arnett 1971; Searle & Sargent 1972), then those proto-Galactic fragments which are similar in luminosity to the Fornax dSph ( $L_V = 1.5 \times 10^7 L_{V,\odot}$ ) galaxy are expected to have contributed roughly half of the number of halo field stars with  $[\text{Fe}/\text{H}] \sim -2$  dex which originated in smaller fragments such as Draco, Sextans and Ursa Minor. Clearly, the measurement of even-Z abundances for stars belonging to the more massive Galactic satellites (such as Fornax, Sagittarius, and Leo I) are urgently needed to test these models.

Alternatively, it may be that the nucleosynthetic history of the proto-Galactic fragments was affected by the building process in such a way as to make them different than the dSph galaxies that survive today. Still another possibility is that the old, gas-poor dSph galaxies sampled here comprised only a small fraction of the actual proto-Galactic fragments, and that the dSph galaxies with younger populations (*i.e.*, those which had more gas for subsequent star formation) show even-Z abundance patterns which more closely resemble those of Galactic halo field stars. Again, element abundances for stars belonging to an expanded sample of dwarf galaxies are required to test these possibilities.

SBS reported that one of their giants, Draco 473, exhibits the deep mixing abundance pattern seen in many globular clusters, with Na enhanced and O and Mg depleted (see Kraft 1994 and Pinsonneault 1997 for recent reviews). With the expanded dSph sample presented here we now reinterpret the abundance pattern of Draco 473 as having its even-Z elements (including O and Mg) not enhanced in comparison to Milky Way halo field stars and probably not due to a deep mixing pattern as originally suggested.

Majewski et al. (2000) have proposed that  $\omega$  Cen may be the nucleus of a dwarf galaxy which has been tidally stripped by the Milky Way. If true, a comparison of the abundances in this dwarf galaxy core to the abundances found in the low luminosity dwarf galaxies sampled here might reveal more clues to the formation of the halo. The dSph galaxies studied here exhibit heavy element abundance patterns which are quite different from those of RGB stars in  $\omega$  Cen: Smith et al. (2000) find a large enhancement of s-process elements relative to r-process elements with increasing metallicity. They attribute this s-process domination to AGB nucleosynthesis enrichment by 1.5-3  $M_\odot$  stars. None of the dSph galaxies in our sample show evidence for such AGB nucleosynthesis enrichment. Thus, if  $\omega$  Cen is indeed the remains of a disrupted dwarf galaxy, then it must have been one different from Draco, Sextans or Ursa Minor. Such a situation would not be entirely surprising given the relative luminosities of the dSph galaxies and  $\omega$  Cen: *i.e.*, the latter has roughly the same luminosity as the three dSph galaxies *combined*. If  $\omega$  Cen is truly the surviving nucleus a dwarf galaxy which has been tidally stripped by the Milky Way, then more massive systems

such as Fornax or Sagittarius may be better analogs for the putative galaxy. Once again, high-resolution abundance analysis for stars belonging to the more massive Galactic satellites are needed to test this possibility.

As noted previously, two of the stars in our sample show large overabundances of the heavy elements with respect to iron and an r-process heavy element abundance pattern. Such stars are known in the Milky Way halo (see Westin et al. 2000; Norris et al. 1997; Cowan et al. 1995), but they are fairly rare. To find two such stars in our small sample suggests that these stars are much more common in dSph environments.

The underabundance of Y in our dSph sample is not easily understood, mainly because Y abundances in the Milky Way nucleosynthesis are themselves poorly understood. We offer two possible solutions and suggest that higher S/N spectra with wider wavelength coverage is required to further understand the first s-process peak. The [Ba/Eu] abundances in Figure 8 suggest that the dSph sample is r-process dominated, at least among the second s-process peak elements. If the first s-process peak were created in a separate site from the second s-process peak, then we might expect to find variations between the various nucleosynthetic sites. Wasserburg et al. (1996) suggest that different r-process sites might exist for low- and high-Z heavy elements, a hypothesis which has some observational support (*e.g.*, Sneden et al. 2000). In an attempt to explain the deep mixing abundance profile found in globular cluster stars, Cavallo & Nagar (2000) suggested that intermediate-mass AGB stars ( $M > 4M_\odot$ ) could produce  $^{27}\text{Al}$  from magnesium. These AGB stars will produce first s-process peak elements but no second s-process peak elements (Denissenkov et al. 1998; Boothroyd & Sackmann 1999). If either of the above processes contributes to the Galactic halo [Y/Fe] abundance pattern, but not to that of dSph stars (or did not contribute to the gas which made up subsequent generations of stars), then the two samples could show different [Y/Fe] ratios. In principal, the contribution of AGB stars could be tested carefully by searching for age spreads within these galaxies.

## 5.2. DLA Comparison

In addition to the samples of dSph and halo stars, Figures 3-8 show element abundances for a sample of DLA systems with low dust contents. Given the complexities of deriving the intrinsic (*i.e.*, undepleted) element abundances in such systems (see, *e.g.*, Vladilo 1998), we show only the observed abundances in these systems, all of which show relatively low levels of dust depletion. For the elements Si, Cr, Mn, and Ni there is agreement among the abundances of the dSph, Milky Way and DLA samples. As is well known, the Zn abundances of the DLA systems are systematically larger than those of the sample of Galactic halo and disk stars; the measured Zn abundances for the dSph stars are smaller still, at least for the more metal-rich dSph stars. The Zn overabundance in DLA systems has sometimes been attributed to depletion of Fe by dust grains (*e.g.*, Pettini et al. 1994; 1999; Kulkarni et al. 1997), although others contend that the usual Zn abundances of the DLA systems may be intrinsic to their stellar nucleosynthesis (Lu et al. 1996).

Obviously, grain depletion is not an issue for our measured dSph abundances. We find significantly different

[Zn/Fe] ratios than in the Galactic halo, suggesting that the mechanism responsible for the production of the Zn in these galaxies was either missing, or was somehow kept from contributing to the enrichment of subsequent generations of stars. The former possibility would suggest that old, low-mass dSph galaxies such as Draco, Ursa Minor and Sextans are not the surviving end-products of high-redshift DLA systems. Alternatively, the latter possibility would indicate that the Zn-rich gas present in these galaxies would have to be removed during a quiescent star formation period, or expelled by an energetic source.

Unfortunately, little is known about the nucleosynthetic site of Zn. Classified as an iron peak element, it is largely ignored in analyses of neutron capture processes. An exception is Burris et al. (2000), who report a solar system r-process fraction of 0.66 for Zn. In light of suggestions that different r-process sites might exist for low- and high-Z heavy elements, a more extensive study of Zn in relation to the first s-process peak elements might provide some useful insights.

## 6. SUMMARY

High-resolution spectra for red giant stars belonging to the Draco, Sextans and Ursa Minor dSph galaxies, and the distant Galactic globular cluster NGC 2419, have been obtained with HIRES on the Keck I telescope. Using these spectra, we have measured element abundances ratios for more than 20 elements. This is the first investigation of the abundance patterns of stars belonging to Sextans, Ursa Minor and NGC 2419, and constitutes a factor of four increase the number of dSph stars having abundances measured from high-resolution spectra.

From a single red giant in NGC 2419, we find a metallicity of  $[\text{Fe}/\text{H}] = -2.32 \pm 0.11$  dex, which is slightly lower than, but in acceptable agreement with, previous estimates from low-resolution spectroscopy (Suntzeff, Kraft & Kinman 1988). With the possible exception of slight enhancements in a number of heavy elements, the measured abundances ratios closely resemble those of red giant stars in M92: a nearby, well-studied globular cluster of similar metallicity.

We find a remarkably uniform abundance pattern for our sample of 17 dSph stars. This suggests that the three dSph galaxies have fairly similar nucleosynthetic histories and, presumably, similar initial mass functions. All three galaxies show unmistakable evidence for a large range in metallicity:  $\Delta[\text{Fe}/\text{H}] = 1.53, 0.73$  and  $1.40$  dex for Draco, Ursa Minor and Sextans, respectively. We find that the dSph stars have  $[\alpha/\text{Fe}]$  abundances which are  $\simeq 0.2$  dex *lower* than those of halo field stars in the same metallicity range: *i.e.*,  $[\alpha/\text{Fe}] \simeq 0.1$  dex, compared to  $[\alpha/\text{Fe}] \simeq 0.3$  dex for halo stars. The measured  $[\text{Eu}/\text{Fe}]$  and  $[\text{Ba}/\text{Fe}]$  abundances for the dSph stars suggest that the chemical evolution in the dSph environments has been dominated by the r-process. In addition, the dSph stars show significantly larger  $[\text{Ba}/\text{Y}]$  abundance ratios than do halo field stars over the full range in metallicity. These observations provide some evidence against the notion that the Galactic halo has been assembled *entirely* through the disruption of very low-luminosity dSph galaxies like the three galaxies studied here. A more detailed assessment of role played by the disruption of dwarf galaxies in the formation of the Galactic halo must await the measurement of

element abundances for stars belonging to an expanded sample of Galactic satellites, particularly more luminous systems such as Sagittarius, Fornax and Leo I.

A comparison of the measured abundance ratios for the dSph stars with those reported for DLA systems having low levels of dust depletion reveals  $[\text{Zn}/\text{Fe}]$  abundance ratios which are nearly an order of magnitude lower than those in the high-redshift absorbers, indicating that old, gas-poor dSph galaxies like those studied here are probably not the low-redshift analogs of the DLA systems.

This work was based on observations obtained at the W.M. Keck Observatory, which is operated jointly by the California Institute of Technology and the University of California. We are grateful to the W.M. Keck Foundation for their vision and generosity. We thank Tom Barlow for helpful advice on the use of MAKEE. We thank Jon Fulbright, Andy McWilliam, John Cowan and Jim Truran for their insightful discussions. Thanks also to Peter Stetson, Kyle Cudworth and Nick Suntzeff for providing photometry for the dwarf galaxies in electronic form. PC acknowledges support provided by the Sherman M. Fairchild Foundation. WLWS was supported by grant AST 99-00733 from the National Science Foundation.

TABLE 1  
OBSERVING LOG

| Run | Date          | Decker | Binning | $\lambda/\Delta\lambda$ | Program Objects            |
|-----|---------------|--------|---------|-------------------------|----------------------------|
| 1   | 13-15/03/1999 | C5     | 1×2     | 34,000                  | Sextans, NGC 2419, M3, M92 |
| 2   | 15-16/07/1999 | C5     | 1×2     | 34,000                  | Ursa Minor, M3, M92        |
| 3   | 14/08/1999    | C5     | 1×2     | 34,000                  | Draco                      |

TABLE 2  
PROPERTIES OF PROGRAM STARS

| Star                  | $V$<br>(mag) | $B - V$<br>(mag) | $E(B - V)$<br>(mag) | $T$<br>(sec) | S/N | HJD<br>(+2450000.0) | $v_r$<br>(km s <sup>-1</sup> ) |
|-----------------------|--------------|------------------|---------------------|--------------|-----|---------------------|--------------------------------|
| <u>M92 = NGC 6341</u> |              |                  |                     |              |     |                     |                                |
| III-13                | 12.03        | 1.31             | 0.02                | 360          | 105 | 1253.10461          | -111.8±0.7                     |
|                       |              |                  |                     | 240          | 93  | 1374.75736          | -114.1±0.3                     |
| VII-18                | 12.19        | 1.28             | 0.02                | 300          | 101 | 1375.75659          | -117.7±0.2                     |
| V-106                 | 12.47        | 1.12             | 0.02                | 300          | 81  | 1375.74965          | -124.0±0.6                     |
| III-65                | 12.49        | 1.17             | 0.02                | 360          | 83  | 1253.11160          | -119.7±0.6                     |
|                       |              |                  |                     | 300          | 88  | 1374.76362          | -119.0±0.3                     |
| <u>M3 = NGC 5272</u>  |              |                  |                     |              |     |                     |                                |
| III-28                | 12.81        | 1.36             | 0.01                | 240          | 65  | 1253.16298          | -152.8±0.2                     |
| I-21                  | 13.05        | 1.36             | 0.01                | 300          | 65  | 1374.74650          | -145.6±0.3                     |
| IV-101                | 13.26        | 1.29             | 0.01                | 480          | 77  | 1375.73520          | -144.8±0.3                     |
| <u>NGC 2419</u>       |              |                  |                     |              |     |                     |                                |
| RH10                  | 17.61        | 1.17             | 0.06                | 3600         | 20  | 1250.77596          | -18.1±0.4                      |
| <u>Draco</u>          |              |                  |                     |              |     |                     |                                |
| 11                    | 17.60        | 1.12             | 0.03                | 3600         | 24  | 1404.82121          | -283.1±0.7                     |
| 343                   | 17.62        | 1.12             | 0.03                | 3600         | 24  | 1404.86929          | -293.1±0.8                     |
| <u>Ursa Minor</u>     |              |                  |                     |              |     |                     |                                |
| 177                   | 16.90        | 1.29             | 0.03                | 3600         | 36  | 1374.79308          | -234.5±0.3                     |
| 297                   | 16.91        | 1.57             | 0.03                | 3600         | 36  | 1374.88445          | -235.9±0.3                     |
| K                     | 16.98        | 1.35             | 0.03                | 3600         | 34  | 1375.82789          | -246.1±0.6                     |
| O                     | 17.03        | 1.31             | 0.03                | 3600         | 34  | 1375.87494          | -250.5±1.1                     |
| 199                   | 17.15        | 1.38             | 0.03                | 3600         | 33  | 1374.83949          | -249.2±0.3                     |
| 168                   | 17.88        | 0.95             | 0.03                | 3600         | 19  | 1375.78264          | -232.9±0.5                     |
| <u>Sextans</u>        |              |                  |                     |              |     |                     |                                |
| S35                   | 17.30        | 1.41             | 0.05                | 3600         | 27  | 1250.92386          | 218.2±0.3                      |
| S56                   | 17.37        | 1.43             | 0.05                | 3600         | 26  | 1250.82948          | 226.9±0.4                      |
| S49                   | 17.59        | 1.15             | 0.05                | 3600         | 17  | 1250.87628          | 230.9±0.6                      |
| S58                   | 17.69        | 1.17             | 0.05                | 3600         | 21  | 1251.77326          | 219.8±0.4                      |
| S36                   | 17.96        | 1.10             | 0.05                | 3600         | 13  | 1252.77161          | 222.9±0.5                      |

STAR IDENTIFICATIONS: Draco – Baade & Swope (1961); Ursa Minor – Van Agt (1967); Sextans – Suntzeff et al. (1993).

REFERENCES FOR PHOTOMETRY: M92 – Sandage & Walker (1966), Sandage (1970); M3 – Johnson & Sandage (1956), Sandage (1953); NGC 2419 – Racine & Harris (1975); Draco – Stetson (2000, private communication); Ursa Minor – Cudworth (2000, private communication); Sextans – Suntzeff et al. (1993).



TABLE 3

| Line<br>(Å) | EP<br>(eV) | log <i>gf</i> | NGC 2419 | Draco |     | Ursa Minor |     |     |     |     |     | Sextans |     |     |     |     |
|-------------|------------|---------------|----------|-------|-----|------------|-----|-----|-----|-----|-----|---------|-----|-----|-----|-----|
|             |            |               | RH10     | 11    | 343 | 177        | 297 | K   | O   | 199 | 168 | S35     | S56 | S49 | S58 | S36 |
| Fe I        |            |               |          |       |     |            |     |     |     |     |     |         |     |     |     |     |
| 5006.12     | 2.83       | -0.628        | 135      | 144   | 135 | 130        | 183 | 131 | 136 | 167 | 121 | 149     | 155 | 92  | 167 | 117 |
| 5083.35     | 0.96       | -2.862        | 169      | 162   | 150 | 150        | 223 |     | 160 |     | 120 | 180     | 179 | 98  | 155 | 170 |
| 5150.85     | 0.99       | -3.030        | 143      | 152   | 137 | 150        | 215 |     | 137 |     | 116 | 169     | 154 | 99  | 178 | 145 |
| 5171.61     | 1.48       | -1.751        | 163      | 165   | 168 | 178        |     | 149 | 177 |     | 144 |         |     | 131 |     | 160 |
| 5216.28     | 1.61       | -2.102        | 133      | 144   | 142 | 144        |     | 136 | 154 |     | 96  | 158     | 145 | 106 | 142 |     |
| 5217.30     | 3.21       | -1.270        | 74       | 95    | 82  | 82         | 125 | 69  | 82  | 112 | 47  | 95      | 87  |     | 92  | 39  |
| 5232.95     | 2.94       | -0.067        | 145      | 170   | 156 | 167        | 228 | 138 | 146 |     | 120 |         | 170 | 102 | 160 | 158 |
| 5250.21     | 0.12       | -4.700        | 119      | 117   | 122 | 133        |     | 100 | 136 |     |     | 159     | 162 |     | 141 | 93  |
| 5253.02     | 2.28       | -3.810        |          |       |     |            | 55  |     | 18  | 46  |     |         | 25  |     | 30  |     |
| 5307.37     | 1.61       | -2.812        | 100      | 107   | 100 | 118        | 162 | 73  | 106 | 138 | 68  | 113     | 141 | 50  | 130 | 85  |
| 5324.19     | 3.21       | -0.100        | 118      | 147   | 124 | 136        |     | 115 | 132 |     | 85  | 135     | 151 | 80  | 168 | 122 |
| 5501.48     | 0.96       | -3.050        | 160      | 149   | 153 | 166        |     | 165 | 169 |     | 100 |         |     | 101 |     | 136 |
| 5506.79     | 0.99       | -2.790        | 163      |       | 134 | 180        |     | 150 | 178 |     | 140 |         |     | 132 |     | 148 |
| 5956.70     | 0.86       | -4.570        | 75       | 87    | 67  | 82         | 159 | 46  | 87  | 134 | 31  | 100     | 114 | 23  | 129 | 67  |
| 5976.79     | 3.94       | -1.290        |          | 41    | 31  | 28         | 57  |     |     | 46  |     |         |     |     |     |     |
| 6027.06     | 4.07       | -1.180        |          | 32    |     | 30         | 53  |     |     | 68  |     | 18      |     |     |     |     |
| 6056.01     | 4.73       | -0.450        |          | 29    |     |            | 50  |     | 20  | 40  | 16  |         |     |     |     |     |
| 6078.50     | 4.79       | -0.370        |          |       |     | 21         | 46  |     | 19  | 40  |     |         |     |     |     |     |
| 6079.01     | 4.65       | -0.950        |          |       |     |            |     |     |     | 25  |     |         |     |     |     |     |
| 6082.72     | 2.22       | -3.590        |          |       |     | 25         | 86  |     | 33  | 73  |     |         |     |     |     |     |
| 6120.26     | 0.91       | -5.940        |          |       |     |            | 40  |     |     | 33  |     |         |     |     |     |     |
| 6136.62     | 2.45       | -1.500        | 133      | 140   | 133 | 141        | 220 | 118 | 141 |     | 87  | 149     | 156 | 64  | 158 | 148 |
| 6137.70     | 2.59       | -1.366        | 132      | 125   | 106 | 123        | 211 | 113 | 134 |     | 81  | 147     | 157 | 54  | 148 | 142 |
| 6151.62     | 2.18       | -3.370        |          | 46    | 34  | 39         | 106 | 19  | 50  | 83  | 17  | 60      | 67  |     | 83  |     |
| 6157.73     | 4.07       | -1.260        |          | 38    |     | 24         | 73  |     | 27  |     |     | 34      |     |     | 37  |     |
| 6165.36     | 4.14       | -1.470        |          |       |     |            | 24  |     |     | 34  |     |         |     |     |     |     |
| 6173.34     | 2.22       | -2.850        | 50       | 82    | 55  | 72         | 130 | 46  | 73  | 115 | 30  | 83      | 80  |     | 97  | 47  |
| 6187.99     | 3.94       | -1.580        |          |       |     |            | 38  |     |     | 48  |     |         |     |     |     |     |
| 6213.43     | 2.22       | -2.660        | 72       |       |     | 100        |     |     | 98  | 123 |     | 119     | 104 |     | 130 | 89  |
| 6229.23     | 2.84       | -2.900        |          | 20    | 21  | 17         | 46  |     |     | 51  |     | 29      | 34  |     | 35  |     |
| 6230.74     | 2.56       | -1.276        | 138      | 163   | 144 | 148        | 227 | 138 | 155 |     | 105 | 167     | 165 | 87  | 148 | 124 |
| 6240.66     | 2.22       | -3.230        |          | 50    | 24  | 47         | 107 |     | 40  | 77  |     | 69      | 65  |     | 59  |     |
| 6252.57     | 2.40       | -1.757        | 137      | 121   | 122 | 135        | 172 | 108 | 139 | 167 | 99  | 144     | 155 | 62  | 138 | 125 |
| 6290.97     | 4.73       | -0.760        |          |       |     |            | 32  |     |     |     |     |         |     |     |     |     |
| 6297.80     | 2.22       | -2.740        |          | 66    | 87  | 105        | 143 |     | 90  | 120 | 57  |         |     |     |     |     |
| 6353.84     | 0.91       | -6.430        |          |       |     |            | 11  |     |     | 11  |     |         |     |     |     |     |
| 6355.04     | 2.84       | -2.290        |          | 62    | 48  | 51         | 123 |     | 58  | 94  |     |         |     |     |     |     |
| 6380.75     | 4.19       | -1.500        |          |       |     |            | 54  |     |     | 42  |     |         |     |     |     |     |
| 6392.54     | 2.28       | -3.950        |          |       | 16  |            | 50  |     |     | 38  |     |         |     |     |     |     |
| 6393.61     | 2.43       | -1.630        |          | 147   | 131 | 129        |     | 155 | 138 | 179 | 82  |         |     |     |     |     |
| 6498.94     | 0.96       | -4.690        |          | 86    | 62  | 64         | 158 | 48  | 80  | 113 |     |         |     |     |     |     |
| 6518.37     | 2.83       | -2.460        |          | 56    | 47  | 44         | 89  | 25  | 38  | 81  |     |         |     |     |     |     |
| 6574.23     | 0.99       | -5.020        |          | 50    | 49  | 53         | 114 | 39  | 48  | 94  |     |         |     |     |     |     |
| 6581.22     | 1.48       | -4.680        |          |       | 33  | 21         | 77  |     | 21  | 59  |     |         |     |     |     |     |
| 6593.88     | 2.43       | -2.390        |          | 82    | 80  | 87         | 143 | 80  | 92  | 138 |     |         |     |     |     |     |
| 6608.03     | 2.28       | -3.940        |          |       |     |            | 40  |     |     | 26  |     |         |     |     |     |     |
| 6609.12     | 2.56       | -2.660        |          | 59    | 44  | 43         | 119 | 44  | 69  | 106 |     |         |     |     |     |     |
| Fe II       |            |               |          |       |     |            |     |     |     |     |     |         |     |     |     |     |
| 5234.63     | 3.22       | -2.118        | 66       | 87    | 84  | 87         | 75  | 88  | 85  | 95  | 65  | 89      | 88  | 75  | 121 | 70  |
| 5264.81     | 3.23       | -3.210        |          | 37    | 31  | 23         | 40  |     | 33  | 48  |     | 30      | 33  |     | 45  | 27  |
| 6149.25     | 3.89       | -2.720        |          | 30    | 25  | 22         | 17  | 23  | 31  | 39  |     | 29      | 20  |     | 40  |     |
| 6369.46     | 2.89       | -4.250        |          |       | 17  |            |     |     |     | 29  |     |         |     |     |     |     |
| 6456.39     | 3.90       | -2.080        |          | 52    | 49  | 46         | 58  | 53  | 50  | 71  | 28  |         |     |     |     |     |
| 6516.08     | 2.89       | -3.450        |          | 58    | 44  | 43         | 44  | 44  | 55  | 59  |     |         |     |     |     |     |
| O I         |            |               |          |       |     |            |     |     |     |     |     |         |     |     |     |     |
| 6363.79     | 0.02       | -10.250       |          | <10   | 14  | <10        | 17  | <10 | <10 | <10 | <10 |         |     |     |     |     |
| Na I        |            |               |          |       |     |            |     |     |     |     |     |         |     |     |     |     |
| 5682.65     | 2.10       | -0.700        | <19      | <15   | <18 | <15        | 73  | <18 | <15 | <12 | <20 | <15     | <8  | <22 | <20 | <19 |
| 5688.21     | 2.10       | -0.370        | <33      | <20   | <20 | 15         | 88  | <20 | <15 | 27  | <30 | 25      | 25  | <20 | <30 | <20 |
| 6154.23     | 2.10       | -1.560        |          |       |     |            | <13 |     |     |     |     |         |     |     |     |     |
| 6160.75     | 2.10       | -1.260        |          |       |     |            | 29  |     |     |     |     |         |     |     |     |     |
| Mg I        |            |               |          |       |     |            |     |     |     |     |     |         |     |     |     |     |
| 4703.00     | 4.33       | -0.520        | 99       | 123   | 120 | 119        | 177 | 124 | 129 | 128 | 102 | 118     | 108 | 88  | 94  |     |
| 5172.70     | 2.71       | -0.390        | 290      | 298   | 293 | 298        | 457 | 280 | 330 | 368 | 259 | 310     | 349 | 235 | 315 | 264 |
| 5183.27     | 2.70       | -0.170        | 386      | 372   | 327 | 376        | 660 | 400 | 400 | 505 | 305 | 453     | 438 | 228 | 362 | 280 |
| Al I        |            |               |          |       |     |            |     |     |     |     |     |         |     |     |     |     |
| 6696.03     | 3.14       | -1.570        |          | <20   | <10 | <10        | <10 | <10 | <14 | <10 | <10 |         |     |     |     |     |
| Si I        |            |               |          |       |     |            |     |     |     |     |     |         |     |     |     |     |

TABLE 3—*Continued*

| Line<br>(Å) | EP<br>(eV) | log <i>gf</i> | NGC 2419 | Draco |     | Ursa Minor |     |     |     |     |     | Sextans |     |     |     |     |
|-------------|------------|---------------|----------|-------|-----|------------|-----|-----|-----|-----|-----|---------|-----|-----|-----|-----|
|             |            |               | RH10     | 11    | 343 | 177        | 297 | K   | O   | 199 | 168 | S35     | S56 | S49 | S58 | S36 |
| 5645.66     | 4.91       | -2.140        |          |       |     |            | <15 |     |     |     |     |         |     |     |     |     |
| 5665.60     | 4.90       | -2.040        | <10      |       | <20 |            | <13 | <25 | <15 | <15 | <18 | <15     |     | <20 | <20 | <22 |
| 5684.52     | 4.93       | -1.650        | <19      | <15   | <16 | 16         | 34  | 23  | 20  | <12 | <15 | 17      | <16 | <20 | <30 | <27 |
| 5772.26     | 5.06       | -1.750        | <15      | <15   | <20 | <12        | <15 | <18 | <20 | <12 | <20 |         | <20 | <20 | <20 | <30 |
| 6145.02     | 5.61       | -1.370        |          |       | <15 | 16         | <12 | <12 |     | 12  |     |         |     |     | <15 |     |
| 6243.82     | 5.61       | -1.270        |          | <12   | <12 |            |     |     |     | <12 |     | <15     | <12 |     | <18 |     |
| 6244.48     | 5.61       | -1.270        |          | <15   |     | <12        | 18  |     | <18 | 15  | <20 | 12      | <15 | <20 | <20 | <22 |
| Ca I        |            |               |          |       |     |            |     |     |     |     |     |         |     |     |     |     |
| 6122.23     | 1.89       | -0.320        | 124      | 138   | 120 | 138        | 188 | 121 | 139 | 165 | 107 | 149     | 142 | 58  | 143 | 130 |
| 6161.30     | 2.52       | -1.270        |          | 29    |     | 22         | 53  |     | 22  | 64  |     | 26      |     |     | 35  | 30  |
| 6166.44     | 2.52       | -1.140        |          | 42    |     | 22         | 63  |     |     | 45  |     | 28      | 40  |     |     | 30  |
| 6169.04     | 2.52       | -0.800        | 27       | 63    | 39  | 42         | 85  | 45  | 40  | 64  |     | 45      | 45  |     | 43  | 28  |
| 6169.56     | 2.52       | -0.480        | 36       | 75    | 47  | 65         | 95  | 52  | 55  | 81  | 21  | 63      | 72  |     | 72  | 50  |
| 6455.60     | 2.52       | -1.290        |          | 22    |     | 17         | 58  |     | 15  | 45  |     |         |     |     |     |     |
| 6499.65     | 2.52       | -0.820        |          | 44    | 42  | 48         | 88  | 58  | 47  | 60  |     |         |     |     |     |     |
| Ti I        |            |               |          |       |     |            |     |     |     |     |     |         |     |     |     |     |
| 4548.76     | 0.83       | -0.290        | 50       |       |     | 69         |     |     | 94  | 106 |     | 98      | 104 |     |     | 44  |
| 4555.49     | 0.85       | -0.430        | 60       |       |     | 63         | 113 | 62  | 64  | 85  | 44  | 67      | 98  |     | 61  |     |
| 4623.10     | 1.74       | 0.166         | 31       | 48    |     | 25         | 75  |     | 39  | 50  |     |         |     |     |     |     |
| 4645.19     | 1.74       | -0.501        | 5        |       |     | 58         |     |     |     |     |     |         | 35  |     |     |     |
| 4656.47     | 0.00       | -1.280        | 103      | 83    | 85  | 87         |     | 51  | 76  | 128 | 45  | 120     | 107 |     | 89  | 40  |
| 4840.87     | 0.90       | -0.450        | 76       | 54    | 39  | 73         | 140 | 34  | 61  | 87  | 33  | 82      | 93  |     | 74  |     |
| 4913.62     | 1.87       | 0.216         |          | 35    |     | 19         | 71  |     |     | 31  |     |         | 42  |     | 29  |     |
| 4997.10     | 0.00       | -2.060        | 46       |       |     | 64         | 151 |     | 69  | 86  |     | 52      | 58  |     | 47  | 60  |
| 5014.24     | 0.81       | 0.910         | 196      | 167   | 139 | 162        | 273 | 135 | 178 | 220 | 100 | 200     | 188 | 60  | 138 | 113 |
| 5016.16     | 0.85       | -0.510        | 54       | 74    | 53  | 80         | 130 | 44  | 77  | 109 | 36  | 76      | 89  |     | 62  | 47  |
| 5064.65     | 0.05       | -0.930        | 114      | 133   | 96  | 113        | 210 | 94  | 124 |     | 67  | 131     | 128 | 31  | 111 | 110 |
| 5113.44     | 1.44       | -0.727        |          |       |     | 18         | 62  |     |     | 25  |     |         |     |     |     |     |
| 5145.47     | 1.46       | -0.518        |          |       |     | 29         | 64  |     |     | 38  |     |         |     |     |     |     |
| 5210.39     | 0.05       | -0.580        | 112      | 118   | 118 | 136        | 221 | 115 | 148 | 164 | 75  | 136     | 176 | 30  | 133 | 84  |
| 5978.54     | 1.87       | -0.440        |          |       |     | 14         | 34  |     | 26  | 30  |     |         |     |     |     |     |
| Ti II       |            |               |          |       |     |            |     |     |     |     |     |         |     |     |     |     |
| 4583.41     | 1.16       | -2.870        |          | 55    |     | 43         | 73  | 35  | 70  | 78  |     | 48      | 42  |     | 40  |     |
| 4636.32     | 1.16       | -3.230        |          | 48    | 52  | 51         | 58  |     | 35  |     |     | 25      |     |     | 45  |     |
| 4657.20     | 1.24       | -2.320        | 53       | 108   | 75  |            | 97  | 67  | 83  | 84  | 50  | 75      | 79  |     | 39  |     |
| 4708.66     | 1.24       | -2.370        | 78       | 77    | 65  | 73         | 85  |     | 80  | 87  |     | 76      | 88  |     | 62  |     |
| 4719.52     | 1.24       | -3.280        |          | 20    | 37  | 30         | 40  |     | 18  | 50  |     |         |     |     |     |     |
| 4798.53     | 1.08       | -2.670        |          | 77    | 73  | 85         | 103 |     | 87  | 101 |     | 82      |     |     |     | 38  |
| 5154.07     | 1.57       | -1.520        | 90       | 96    | 82  | 104        | 95  | 100 | 100 | 132 | 60  | 105     | 102 | 40  | 95  | 75  |
| 5226.55     | 1.57       | -1.000        | 105      | 115   | 91  | 119        | 152 | 117 | 125 | 135 | 105 | 120     | 125 | 74  | 117 | 100 |
| 5381.01     | 1.57       | -1.780        | 79       | 80    | 72  | 84         | 135 | 76  | 84  | 120 | 45  | 123     | 90  | 45  | 81  | 65  |
| 5418.77     | 1.58       | -2.110        | 74       | 87    | 57  | 70         | 88  | 65  | 86  | 69  | 47  | 69      | 52  | 19  | 63  | 46  |
| V I         |            |               |          |       |     |            |     |     |     |     |     |         |     |     |     |     |
| 6216.37     | 0.28       | -1.270        |          |       | 18  |            | 86  |     | 18  | 35  |     | 24      | 26  |     |     |     |
| 6224.51     | 0.29       | -1.820        |          |       |     |            | 29  |     |     | 23  |     |         |     |     |     |     |
| 6233.20     | 0.28       | -2.000        |          |       |     |            |     |     |     |     |     |         | 11  |     |     |     |
| 6274.66     | 0.27       | -1.690        |          |       |     |            | 57  |     |     |     |     |         |     |     |     |     |
| 6285.16     | 0.28       | -1.560        |          |       |     |            | 75  |     |     |     |     |         |     |     |     |     |
| 6292.82     | 0.29       | -1.520        |          |       |     |            |     |     | 25  | 39  |     |         |     |     |     |     |
| Cr I        |            |               |          |       |     |            |     |     |     |     |     |         |     |     |     |     |
| 5409.80     | 1.03       | -0.720        | 111      | 136   | 100 | 125        | 221 | 119 | 124 | 177 | 59  | 139     | 148 | 40  | 138 | 100 |
| Mn I        |            |               |          |       |     |            |     |     |     |     |     |         |     |     |     |     |
| 5407.42     | 2.14       | -1.743        |          |       |     | 16         | 52  |     |     | 48  |     |         |     |     | 25  | <20 |
| 5420.36     | 2.14       | -1.460        | 13       | <18   |     | 23         | 89  | <20 | 30  | 66  | <20 | 35      | 31  |     |     |     |
| 5432.55     | 0.00       | -3.795        | 30       | 45    | 38  | 34         | 165 | 26  | 51  |     | 21  | 75      | 50  | <20 | 55  | <20 |
| 5516.77     | 2.18       | -1.847        |          |       |     |            | 50  |     |     | 23  |     |         |     |     |     |     |
| 6013.51     | 3.07       | -0.252        | <12      | <15   | 16  | 14         | 54  | <25 | <25 | 51  | <23 | 20      | <18 | <20 | 37  | <20 |
| 6021.82     | 3.08       | 0.035         | 42       | 46    | <18 | 31         | 93  | 30  | 49  | 64  | <24 | 35      | 40  | <27 | 53  | <25 |
| Co I        |            |               |          |       |     |            |     |     |     |     |     |         |     |     |     |     |
| 5483.34     | 1.71       | -1.488        | <23      | 33    | 25  | 54         | 130 | <23 | 34  | 61  | <18 | 39      | 49  | <30 | 22  | <23 |
| 5647.23     | 2.28       | -1.560        |          |       |     | <15        | 18  |     |     | 15  |     |         |     |     |     |     |
| 6454.99     | 3.63       | -0.250        |          |       |     |            | 19  |     |     |     |     |         |     |     |     |     |
| Ni I        |            |               |          |       |     |            |     |     |     |     |     |         |     |     |     |     |
| 5476.92     | 1.83       | -0.890        | 142      | 138   | 137 | 148        | 205 | 134 | 148 | 200 | 110 | 164     | 158 | 116 | 147 | 123 |
| 6176.82     | 4.09       | -0.430        |          |       |     | 20         | 25  |     |     | 22  |     |         |     |     |     |     |



TABLE 4  
ELEMENT ABUNDANCES FOR PROGRAM STARS

| Star                  | T <sub>eff</sub><br>(K) | log <i>g</i><br>(dex) | <i>v<sub>t</sub></i><br>(km s <sup>-1</sup> ) | [Fe/H]<br>(dex) | [O/Fe]<br>(dex) | [Na/Fe]<br>(dex) | [Mg/Fe]<br>(dex) | [Al/Fe]<br>(dex) | [Si/Fe]<br>(dex) | [Ca/Fe]<br>(dex) | [Ti/Fe]<br>(dex) |
|-----------------------|-------------------------|-----------------------|---|-----------------|-----------------|------------------|------------------|------------------|------------------|------------------|------------------|
| <u>M92 = NGC 6341</u> |                         |                       |   |                 |                 |                  |                  |                  |                  |                  |                  |
| III-13                | 4175                    | 0.20                  | 2.10  | -2.28±0.11      | 0.13±0.15       | 0.48±0.10        | 0.64±0.16        | 0.90±0.15        | 0.47±0.15        | 0.30±0.08        | 0.39±0.07        |
| VII-18                | 4225                    | 0.00                  | 2.15  | -2.27±0.11      | <0.15           | 0.38±0.15        | 0.37±0.15        | 1.25±0.15        | 0.75±0.18        | 0.29±0.08        | 0.32±0.07        |
| V-106                 | 4375                    | 0.70                  | 2.00  | -2.33±0.11      | <0.36           | -0.21±0.15       | 0.48±0.15        | <0.90            | 0.47±0.15        | 0.26±0.08        | 0.24±0.07        |
| III-65                | 4325                    | 0.50                  | 2.10  | -2.30±0.11      | 0.23±0.15       | 0.31±0.14        | 0.38±0.18        | 1.01±0.18        | 0.62±0.20        | 0.27±0.07        | 0.15±0.06        |
| <u>M3 = NGC 5272</u>  |                         |                       |   |                 |                 |                  |                  |                  |                  |                  |                  |
| III-28                | 4175                    | 0.70                  | 1.90  | -1.70±0.11      | 0.37±0.14       | -0.23±0.09       | 0.41±0.15        | -0.06±0.20       | 0.31±0.12        | 0.28±0.08        | 0.37±0.07        |
| I-21                  | 4200                    | 0.70                  | 1.70  | -1.44±0.11      | 0.21±0.14       | -0.26±0.09       | 0.30±0.15        | 0.24±0.14        | 0.15±0.14        | 0.27±0.07        | 0.32±0.06        |
| IV-101                | 4225                    | 0.80                  | 1.70  | -1.44±0.11      | 0.02±0.14       | 0.20±0.09        | 0.24±0.13        | 0.85±0.12        | 0.09±0.15        | 0.28±0.08        | 0.32±0.07        |
| <u>NGC 2419</u>       |                         |                       |   |                 |                 |                  |                  |                  |                  |                  |                  |
| RH10                  | 4275                    | 0.70                  | 2.10  | -2.32±0.11      |                 | <0.26            | 0.30±0.18        |                  | <0.72            | 0.11±0.12        | 0.22±0.11        |
| <u>Draco</u>          |                         |                       |   |                 |                 |                  |                  |                  |                  |                  |                  |
| 11                    | 4475                    | 0.80                  | 1.80  | -1.72±0.11      | <0.38           | <-0.34           | 0.07±0.15        | <0.71            | <0.30            | 0.16±0.08        | 0.09±0.07        |
| 343                   | 4475                    | 0.90                  | 1.80  | -1.86±0.11      | 0.42±0.22       | -0.15±0.00       | 0.06±0.20        | <0.34            | <0.50            | 0.03±0.11        | -0.03±0.11       |
| 473                   | 4400                    | 0.90                  | 1.75  | -1.44±0.07      | -0.32±0.18      | -0.04±0.09       | -0.19±0.17       |                  | <0.14            | 0.18±0.08        | -0.18±0.25       |
| 267                   | 4180                    | 0.60                  | 1.95  | -1.67±0.13      | 0.21±0.11       | -0.59±0.17       | -0.04±0.21       |                  | <0.29            | 0.19±0.08        | 0.02±0.31        |
| 24                    | 4290                    | 0.80                  | 2.00  | -2.36±0.09      | 0.38±0.18       | -0.33±0.18       | 0.26±0.16        |                  |                  | 0.07±0.06        | -0.04±0.18       |
| 119                   | 4370                    | 0.15                  | 2.80  | -2.97±0.15      |                 | -0.09±0.17       | 0.20±0.17        |                  |                  | 0.11±0.07        | -0.17±0.31       |
| <u>Ursa Minor</u>     |                         |                       |   |                 |                 |                  |                  |                  |                  |                  |                  |
| 177                   | 4300                    | 0.40                  | 1.90  | -2.01±0.11      | <0.33           | -0.37±0.18       | 0.32±0.17        | <0.68            | 0.51±0.30        | 0.18±0.08        | 0.15±0.08        |
| 297                   | 4075                    | 0.40                  | 2.30  | -1.68±0.11      | 0.18±0.22       | 0.15±0.12        | 0.24±0.22        | <0.21            | 0.30±0.20        | 0.02±0.08        | 0.12±0.07        |
| K                     | 4325                    | 0.10                  | 2.00  | -2.17±0.12      | <0.38           | <0.20            | 0.69±0.25        | <0.90            | <0.88            | 0.43±0.11        | 0.04±0.10        |
| O                     | 4325                    | 0.30                  | 1.80  | -1.91±0.11      | <0.22           | <-0.24           | 0.43±0.20        | <0.51            | 0.32±0.30        | 0.09±0.08        | 0.20±0.07        |
| 199                   | 4325                    | 0.30                  | 1.95  | -1.45±0.11      | <-0.05          | <-0.66           | 0.02±0.17        | <0.01            | 0.00±0.20        | -0.01±0.09       | -0.08±0.09       |
| 168                   | 4625                    | 1.30                  | 1.70  | -2.18±0.12      |                 | <0.30            | 0.23±0.17        |                  | <0.89            | 0.11±0.30        | 0.01±0.14        |
| <u>Sextans</u>        |                         |                       |   |                 |                 |                  |                  |                  |                  |                  |                  |
| S35                   | 4225                    | 0.10                  | 2.00  | -1.93±0.11      |                 | -0.24±0.18       | 0.27±0.19        |                  | 0.45±0.30        | 0.11±0.10        | 0.07±0.10        |
| S56                   | 4175                    | 0.30                  | 1.90  | -1.93±0.11      |                 | -0.27±0.18       | 0.23±0.19        |                  | <0.45            | 0.08±0.10        | 0.13±0.10        |
| S49                   | 4325                    | 0.10                  | 2.50  | -2.85±0.13      |                 |                  | 0.41±0.20        |                  |                  | 0.08±0.23        | -0.29±0.15       |
| S58                   | 4525                    | 1.00                  | 1.90  | -1.45±0.12      |                 | <-0.43           | -0.46±0.19       |                  | <0.30            | -0.12±0.10       | -0.35±0.10       |
| S36                   | 4425                    | 1.10                  | 2.10  | -2.19±0.12      |                 | <0.15            | -0.07±0.20       |                  |                  | 0.34±0.11        | -0.10±0.11       |

TABLE 4 CONT'D  
ELEMENT ABUNDANCES FOR PROGRAM STARS

| Star                  | [Fe/H]<br>(dex) | [V/Fe]<br>(dex) | [Cr/Fe]<br>(dex) | [Mn/Fe]<br>(dex) | [Co/Fe]<br>(dex) | [Ni/Fe]<br>(dex) | [Cu/Fe]<br>(dex) | [Zn/Fe]<br>(dex) | [Cr/Co]<br>(dex) |
|-----------------------|-----------------|-----------------|------------------|------------------|------------------|------------------|------------------|------------------|------------------|
| <u>M92 = NGC 6341</u> |                 |                 |                  |                  |                  |                  |                  |                  |                  |
| III-13                | -2.28±0.11      | 0.04±0.10       | -0.15±0.12       | -0.27±0.08       | 0.18±0.10        | 0.04±0.12        | -0.64±0.15       | 0.17±0.14        | 0.33±0.16        |
| VII-18                | -2.27±0.11      | -0.02±0.12      | -0.10±0.12       | -0.37±0.09       | 0.08±0.10        | 0.02±0.12        | -0.65±0.15       | 0.30±0.16        | 0.18±0.16        |
| V-106                 | -2.33±0.11      | 0.43±0.20       | -0.23±0.14       | -0.28±0.14       | 0.05±0.11        | 0.13±0.13        | -0.76±0.15       | 0.14±0.12        | 0.28±0.18        |
| III-65                | -2.30±0.11      | 0.17±0.10       | -0.27±0.11       | -0.42±0.14       | 0.15±0.15        | 0.10±0.12        | -0.78±0.15       | 0.07±0.12        | 0.42±0.19        |
| <u>M3 = NGC 5272</u>  |                 |                 |                  |                  |                  |                  |                  |                  |                  |
| III-28                | -1.70±0.11      | 0.12±0.09       | -0.01±0.13       | -0.26±0.08       | -0.04±0.20       | 0.11±0.13        | -0.37±0.13       | 0.09±0.14        | -0.03±0.24       |
| I-21                  | -1.44±0.11      | 0.08±0.09       | 0.08±0.12        | -0.14±0.10       | -0.08±0.16       | -0.04±0.12       | -0.17±0.13       | -0.02±0.15       | -0.16±0.20       |
| IV-101                | -1.44±0.11      | 0.08±0.09       | 0.12±0.13        | -0.19±0.10       | 0.07±0.14        | -0.07±0.16       | -0.28±0.13       | 0.05±0.10        | -0.05±0.19       |
| <u>NGC 2419</u>       |                 |                 |                  |                  |                  |                  |                  |                  |                  |
| RH10                  | -2.32±0.11      |                 | -0.32±0.17       | -0.31±0.12       | <0.00            | 0.00±0.19        | <-0.43           | <0.15            |                  |
| <u>Draco</u>          |                 |                 |                  |                  |                  |                  |                  |                  |                  |
| 11                    | -1.72±0.11      |                 | -0.01±0.17       | -0.50±0.10       | -0.19±0.18       | 0.00±0.15        | <-0.35           | -0.21±0.15       | -0.18±0.25       |
| 343                   | -1.86±0.11      | -0.02±0.18      | -0.49±0.18       | -0.56±0.10       | -0.20±0.18       | -0.06±0.21       | <-0.43           | -0.28±0.30       | 0.29±0.25        |
| 473                   | -1.44±0.07      | -0.68±0.18      | -0.05±0.12       | -0.32±0.15       | 0.12±0.14        | 0.19±0.13        | <-0.10           | 0.12±0.20        | 0.17±0.18        |
| 267                   | -1.67±0.13      | -0.20±0.18      | -0.05±0.13       | -0.28±0.16       | <0.05            | 0.36±0.14        | <-0.39           | <-0.46           |                  |
| 24                    | -2.36±0.09      |                 | 0.04±0.11        | <0.05            | -0.07±0.20       | 0.31±0.16        | <-0.15           | 0.10±0.20        | -0.11±0.23       |
| 119                   | -2.97±0.15      |                 | -0.54±0.08       | <0.80            | <1.27            | -0.42±0.11       | <0.92            | <1.06            |                  |
| <u>Ursa Minor</u>     |                 |                 |                  |                  |                  |                  |                  |                  |                  |
| 177                   | -2.01±0.11      |                 | -0.23±0.17       | -0.37±0.10       | 0.26±0.13        | 0.08±0.17        | <-0.50           | -0.01±0.15       | 0.49±0.21        |
| 297                   | -1.68±0.11      | -0.13±0.10      | 0.14±0.18        | -0.35±0.10       | 0.06±0.20        | -0.12±0.15       | <-0.52           | -0.20±0.30       | -0.08±0.27       |
| K                     | -2.17±0.12      |                 | -0.01±0.22       | -0.32±0.18       | <0.10            | -0.02±0.22       | <-0.26           | 0.06±0.20        |                  |
| O                     | -1.91±0.11      | -0.01±0.21      | -0.26±0.17       | -0.33±0.12       | -0.15±0.18       | 0.00±0.17        | <-0.61           | 0.50±0.20        | 0.11±0.25        |
| 199                   | -1.45±0.11      | -0.17±0.11      | 0.07±0.16        | -0.36±0.08       | -0.27±0.15       | -0.18±0.25       | <-0.80           | -0.26±0.25       | -0.34±0.22       |
| 168                   | -2.18±0.12      |                 | -0.64±0.23       | <-0.10           | <0.17            | 0.03±0.22        | <0.10            | 0.03±0.15        |                  |
| <u>Sextans</u>        |                 |                 |                  |                  |                  |                  |                  |                  |                  |
| S35                   | -1.93±0.11      | -0.26±0.18      | -0.27±0.20       | -0.46±0.10       | -0.20±0.20       | 0.01±0.20        | <-0.74           | -0.15±0.30       | 0.07±0.28        |
| S56                   | -1.93±0.11      | -0.22±0.15      | -0.18±0.19       | -0.66±0.12       | -0.14±0.20       | -0.08±0.19       | <-0.78           | -0.10±0.20       | 0.04±0.28        |
| S49                   | -2.85±0.13      |                 | -0.46±0.23       |                  |                  | 0.26±0.23        |                  | <0.47            |                  |
| S58                   | -1.45±0.12      |                 | -0.29±0.24       | -0.49±0.10       | -0.64±0.30       | -0.33±0.24       | <-0.58           | -0.56±0.30       | -0.35±0.38       |
| S36                   | -2.19±0.12      |                 | -0.38±0.23       | <-0.14           | <0.10            | -0.24±0.23       | <0.10            | -0.02±0.25       |                  |

TABLE 4 CONT'D  
ELEMENT ABUNDANCES FOR PROGRAM STARS

| Star                  | [Fe/H]<br>(dex) | [Y/Fe]<br>(dex) | [Ba/Fe]<br>(dex) | [Ce/Fe]<br>(dex) | [Nd/Fe]<br>(dex) | [Sm/Fe]<br>(dex) | [Eu/Fe]<br>(dex) | [Ba/Eu]<br>(dex) | [Ba/Y]<br>(dex) |
|-----------------------|-----------------|-----------------|------------------|------------------|------------------|------------------|------------------|------------------|-----------------|
| <u>M92 = NGC 6341</u> |                 |                 |                  |                  |                  |                  |                  |                  |                 |
| III-13                | -2.28±0.11      | -0.25±0.07      | -0.50±0.07       | -0.57±0.10       | -0.37±0.10       | 0.08±0.14        | -0.04±0.14       | -0.46±0.16       | -0.25±0.10      |
| VII-18                | -2.27±0.11      | -0.35±0.07      | -0.50±0.07       | -0.51±0.10       | -0.28±0.10       | 0.02±0.14        | -0.03±0.14       | -0.47±0.16       | -0.15±0.10      |
| V-106                 | -2.33±0.11      | -0.33±0.07      | -0.40±0.07       | -0.50±0.10       | -0.14±0.10       | 0.12±0.14        | 0.27±0.14        | -0.67±0.16       | -0.07±0.10      |
| III-65                | -2.30±0.11      | -0.41±0.07      | -0.43±0.07       | -0.47±0.10       | -0.16±0.10       | 0.27±0.14        | 0.16±0.14        | -0.59±0.16       | -0.02±0.10      |
| <u>M3 = NGC 5272</u>  |                 |                 |                  |                  |                  |                  |                  |                  |                 |
| III-28                | -1.70±0.11      | 0.08±0.07       | 0.08±0.07        | -0.15±0.10       | 0.28±0.10        | 0.63±0.14        | 0.48±0.14        | -0.40±0.16       | 0.00±0.10       |
| I-21                  | -1.44±0.11      | -0.16±0.07      | 0.05±0.07        | -0.19±0.10       | 0.17±0.10        | 0.29±0.14        | 0.38±0.14        | -0.33±0.16       | 0.21±0.10       |
| IV-101                | -1.44±0.11      | -0.08±0.07      | 0.14±0.07        | 0.06±0.10        | 0.29±0.10        | 0.47±0.14        | 0.40±0.14        | -0.26±0.16       | 0.22±0.10       |
| <u>NGC 2419</u>       |                 |                 |                  |                  |                  |                  |                  |                  |                 |
| RH10                  | -2.32±0.11      | 0.03±0.10       | -0.15±0.10       | -0.05±0.14       | 0.19±0.14        | <0.80            |                  |                  | -0.18±0.14      |
| <u>Draco</u>          |                 |                 |                  |                  |                  |                  |                  |                  |                 |
| 11                    | -1.72±0.11      | -0.68±0.10      | 0.11±0.10        | -0.13±0.14       | 0.23±0.14        | 0.36±0.20        | 0.55±0.20        | -0.44±0.22       | 0.79±0.14       |
| 343                   | -1.86±0.11      | -0.45±0.10      | 0.09±0.10        | -0.53±0.14       | -0.19±0.14       | 0.18±0.20        | 0.51±0.20        | -0.42±0.22       | 0.54±0.14       |
| 473                   | -1.44±0.07      | -0.74±0.16      | -0.01±0.16       | 0.03±0.35        | 0.50±0.35        |                  |                  |                  | 0.73±0.23       |
| 267                   | -1.67±0.13      | -0.73±0.16      | 0.41±0.16        | 0.19±0.35        | 0.11±0.18        |                  |                  |                  | 1.14±0.23       |
| 24                    | -2.36±0.09      | <-0.65          | -1.19±0.25       | <0.00            | <-0.04           |                  |                  |                  |                 |
| 119                   | -2.97±0.15      | <-0.39          | <-1.17           | <0.41            | <0.37            |                  |                  |                  |                 |
| <u>Ursa Minor</u>     |                 |                 |                  |                  |                  |                  |                  |                  |                 |
| 177                   | -2.01±0.11      | -0.52±0.10      | -0.22±0.10       | -0.51±0.14       | -0.09±0.14       | 0.48±0.20        | 0.26±0.20        | -0.48±0.22       | 0.30±0.14       |
| 297                   | -1.68±0.11      | -0.04±0.09      | 0.15±0.09        | -0.23±0.11       | 0.45±0.11        | 1.06±0.18        | 0.74±0.18        | -0.59±0.20       | 0.19±0.13       |
| K                     | -2.17±0.12      | 0.06±0.09       | 1.37±0.09        | 1.36±0.11        | 1.28±0.11        | 1.73±0.18        | 1.04±0.18        | 0.33±0.20        | 1.31±0.13       |
| O                     | -1.91±0.11      | -0.67±0.10      | -0.39±0.10       | -1.02±0.14       | -0.27±0.14       | 0.28±0.20        | 0.15±0.20        | -0.54±0.22       | 0.28±0.14       |
| 199                   | -1.45±0.11      | 0.34±0.09       | 0.77±0.09        | 1.03±0.11        | 1.13±0.11        | 1.75±0.18        | 1.49±0.18        | -0.72±0.20       | 0.43±0.13       |
| 168                   | -2.18±0.12      | -0.34±0.10      | 0.18±0.09        | -0.18±0.14       | 0.23±0.14        | <0.65            | <1.30            |                  | 0.52±0.13       |
| <u>Sextans</u>        |                 |                 |                  |                  |                  |                  |                  |                  |                 |
| S35                   | -1.93±0.11      | -0.07±0.10      | 0.70±0.10        | 0.89±0.11        | 0.79±0.11        | 1.58±0.18        |                  |                  | 0.77±0.14       |
| S56                   | -1.93±0.11      | -0.37±0.13      | 0.23±0.14        | -0.25±0.14       | 0.22±0.14        | 0.86±0.20        |                  |                  | 0.60±0.19       |
| S49                   | -2.85±0.13      | <-0.35          | -1.05±0.15       | <0.45            | <0.50            | <0.94            |                  |                  |                 |
| S58                   | -1.45±0.12      | -0.77±0.13      | 0.11±0.14        | -0.54±0.14       | 0.00±0.14        | 0.52±0.20        |                  |                  | 0.88±0.19       |
| S36                   | -2.19±0.12      | 0.25±0.13       | 0.39±0.14        | <0.46            | 0.52±0.14        | <1.34            |                  |                  | 0.14±0.19       |

## REFERENCES

- Aaronson, M., Hodge, P. W., & Olszewski, E. W. 1983, *ApJ*, 267, 271
- Armandroff, T.E., Olszewski, E.W., & Pryor, C. 1995, *AJ*, 110, 2131
- Armosky, B.J., Sneden, C., Langer, G.E., & Kraft, R.P. 1994, *AJ*, 108, 1364
- Baade, W., & Swope, H. 1961, *AJ*, 84, 1149
- Bergbusch, P.A., & Vandenberg, D.A. 1992, *ApJS*, 81, 163
- Bizzarri, A., Huber, M.C.E., Noels, A., Greves, N., Bergeson, S.D., Tsekeris, P., & Lawler, J.E. 1993, *A&A*, 273, 707
- Blackwell, D.E., Petford, A.D., Shallis, M.J., & Leggett, S. 1982, *MNRAS*, 199, 21
- Blackwell, D.E., Booth, A. J., Menon, S.L.R., & Petford, A.D. 1986, *MNRAS*, 220, 289
- Blitz, L., & Robishaw, T. 2000, *ApJ*, in press (astro-ph/0001142)
- Boothroyd, A.I., & Sackmann, I.J. 1999, *ApJ*, 510, 232
- Briley, M.M., Smith, V.V., Suntzeff, N.B., Lambert, D.L., Bell, R.A., & Hesser, J.E. 1995, *Nature*, 383, 604
- Burris, D.L., Pilachowski, C.A., Armandroff, T.E., Sneden, C., Cowan, J.J., & Roe, H. 2000, *AJ*, submitted (astro-ph/0005188)
- Canterna, R. 1975, *ApJ*, 200, 63
- Canterna, R., & Schommer, R. A. 1978, *ApJ*, 219, 119
- Carretta, E., & Gratton, R. G. 1997, *A&AS*, 121, 95
- Cathey, L. 1974, *AJ*, 79, 1370
- Cavallo, R.M., Sweigart, A.V., & Bell, R.A. 1996, *ApJ*, 464, L79
- Cavallo, R.M., & Nagar, N.M. 2000, *AJ*, in press (astro-ph/0002511)
- Côté, P., Oke, J.B., & Cohen, J.G. 1999, *AJ*, 118, 1645
- Côté, P., Marzke, R.O., West, M.J., & Minniti, D. 2000, *ApJ*, 533, 869
- Cowan, J.J., Burris, D.L., Sneden, C., McWilliam, A., & Preston, G.W. 1995, *ApJ*, 439, 51
- Da Costa, G.S., Hatzidimitriou, D., Irwin, M.J., & McMahon, R.G. 1991, *MNRAS*, 249, 473
- Da Costa, G.S., Armandroff, T.E., Caldwell, N., & Seitzer, P. 2000, *AJ*, 119, 705
- Denissenkov, P.A., Da Costa, G.S., Norris, J.E., & Weiss, A. *A&A*, 333, 926
- Edvardsson, B., Andersen, J., Gustafsson, B., Lambert, D.L., Nissen, P.E., & Tomkin, J. 1993, *A&A*, 275, 101 (E93)
- Fuhrmann, K., Axer, M., & Gehren, T. 1995, *A&A*, 301, 492
- Gallagher, J.S., & Wyse, R.F.G. 1994 *PASP*, 106, 1225
- Gratton, R.G. 1989, *A&A*, 208, 171 (GS)
- Gratton, R.G., & Sneden, C. 1988, *A&A*, 204, 193 (GS)
- Gratton, R.G., & Sneden, C. 1991, *A&A*, 241, 501 (GS)
- Gratton, R.G., & Sneden, C. 1994, *A&A*, 287, 927 (GS)
- Grebel, E.K. 1999, in *The Stellar Content of Local Group Galaxies*, IAU Symposium 192, eds P. Whitelock & R. Cannon, (San Francisco, ASP), p. 17
- Grillmair, C.J., et al. 1998, *AJ*, 115, 144
- Gustafsson, B., Bell, R.A., Erickson, K., & Norlund, A. 1975, *A&A*, 42, 407
- Haehnelt, M.G., Steinmetz, M., & Rauch, M. 1998, *ApJ*, 495, 647
- Haehnelt, M.G., Steinmetz, M., & Rauch, M. 2000, *ApJ*, 534, 594
- Hernandez, X., Gilmore, G., & Valls-Gabaud, D. 2000, *MNRAS*, in press (astro-ph/0001337)
- Hilker, M., & Richtler, T. 2000, in *Proc. Liege Int. Astrophys. Coll., The Galactic Halo: From Globular Clusters to Field Stars*, ed. A. Noels et al., in press (astro-ph/9910370)
- Hodge, P.W. 1971, *ARA&A*, 9, 35
- Hughes, J., & Wallerstein, G. 2000, *AJ*, 119, 1225
- Ibata, R.A., Gilmore, G., & Irwin, M.J. 1994, *Nature*, 370, 194
- Evans, I.I., Carney, B., de Almeida, L., & Sneden, C. 2000, in *Dynamics of Star Clusters and the Milky Way*, ASP Conf. Ser., in press
- Johnson, H., & Sandage, A. 1956, *ApJ*, 124, 379
- Kraft, R.P. Sneden, C., Langer, G.E., & Prosser, C.F. 1992, *AJ*, 104, 645
- Kraft, R.P. Sneden, C., Langer, G.E., & Shetrone, M.D. 1993, *AJ*, 106, 1490
- Kraft, R.P. 1994, *PASP*, 106, 553
- Kraft, R.P. Sneden, C., Langer, G.E., Shetrone, M.D., & Bolte, M. 1995, *AJ*, 109, 2586
- Kraft, R. P., Sneden, C., Smith, G.H., Shetrone, M.D., Langer, G.E., & Pilachowski, C. A. 1996, *AJ*, 113, 279
- Kraft, R. P., Sneden, C., Smith, G. H., Shetrone, M. D., Langer, G. E., & Pilachowski, C. A. 1997, *AJ*, 113, 279
- Klypin, A.A., Kravtsov, A.V., Valenzuela, O., & Prada, F. 1999, *ApJ*, 522, 82
- Kulkarni, V. P., Fall, S. M., & Truran, J. W. 1997, *ApJ*, 484, 7
- Larson, R.B. 1988, in *Globular Cluster Systems in Galaxies*, IAU Symposium 126, edited by G. Grindlay and A. Philip (Dordrecht: Kluwer), 311
- Langer, G.E., Hoffman, R.D., & Zaidins, C.S. 1997, *PASP*, 109, 244
- Larson, R.B. 1988, in *Globular Cluster Systems in Galaxies*, IAU Symposium 126, edited by G. Grindlay and A. Philip (Dordrecht: Kluwer), 311
- Lehnert, M.D., Bell, R.A., Hesser, J.E., & Oke, J.B. 1992, *ApJ*, 395, 466
- Lu, L., Sargent, W. L. W., Barlow, T. A., Churchill, C. W., & Vogt, S. S. 1996, *ApJS*, 107, 475
- Majewski, S. R., Patterson, R. J., Dinescu, D. I., Johnson, W. Y., Osthimer, J. C., Kunkel, W. E., & Palma, C. 2000, in *Proc. Liege Int. Astrophys. Coll., The Galactic Halo: From Globular Clusters to Field Stars*, ed. A. Noels et al., in press (astro-ph/9910278)
- Mateo, M., Fischehr, P., & Krzeminski, W. 1995, *AJ*, 110, 2166
- Mateo, M. 1996, in *Formation of the Galactic Halo... Inside and Out*, ASP Conference Series, Vol. 92, edited by H. Morrison and A. Sarajedini (San Francisco: ASP), 434
- Mateo, M. 1998, *ARA&A*, 36, 435
- McWilliam, A., Preston, G.W., Sneden, C., & Searle, L. 1995, *AJ*, 109, 2757 (M95)
- McWilliam, A., & Rich, M. 1994, *ApJS*, 91, 749
- McWilliam, A. *ARA&A*, 35, 503
- Moore, B., Ghinga, S., Governato, F., Lake, G., Quinn, T., Stadel, J., & Tozzi, P. 1999, *ApJ*, 524, 19
- Nissen, P.E., & Schuster, W.J. 1997, *A&A*, 326, 751 (NS)
- Norris, J.E., Ryan, S.G., & Beers, T.C. 1997, *ApJ*, 489, 169
- Olszewski, E.W., Aaronson, M., & Hill, J.M. 1995, *AJ*, 110, 2120
- Pancino, E., Ferraro, F.R., Bellazzini, M., Piotto, G., & Zoccali, M. 2000, *ApJ*, 534, 83
- Pettini, M., Smith, L.J., Hunstead, R.W., & King, D. L. 1994, *ApJ*, 426, 79
- Pettini, M., Smith, L.J., King, D.L., & Hunstead, R.W. 1997, *ApJ*, 486, 665
- Pettini, M., Boksenberg, A., & Hunstead, R.W. 1990, *ApJ*, 348, 48
- Pettini, M., Ellison, S.L., Steidel, C.C., & Bowen, D.V. 1999, *ApJ*, 510, 576
- Pettini, M., Ellison, S.L., Steidel, C.C., Shapley, A.E., & Bowen, D.V. 2000, *ApJ*, 532, 65 (P00)
- Pilachowski, C. A., Sneden, C., & Kraft, R. P. 1996, *AJ*, 111, 1689
- Pinsonneault, M. 1997, *ARA&A*, 35, 557
- Prochaska, J.X., & Wolfe, A.M. 1997, *ApJ*, 487, 73
- Racine, R., & Harris, W.E. 1975, *ApJ*, 196, 413
- Sandage, A. 1953, *AJ*, 58, 61
- Sandage, A. 1970, *ApJ*, 162, 841
- Sandage, A., & Walker, M. 1966, *ApJ*, 143, 313
- Schlegel, D.J., Finkbeiner, D.P., & Davis, M. 1998, *ApJ*, 500, 525
- Searle, L., & Sargent, W.L.W. 1972, *ApJ*, 173, 25
- Searle, L., & Zinn, R. 1978, *ApJ*, 225, 357
- Shetrone, M.D. 1994, *PASP*, 106, 161
- Shetrone, M.D. 1996, *AJ*, 112, 1517
- Shetrone, M.D., Bolte, M., & Stetson, P.B. 1998, *AJ*, 115, 1888 (SBS)
- Smith, V.V., Suntzeff, N.B., Cunha, K., Gallino, R., Busso, M., Lambert, D.L., & Straniero, O. 2000, *AJ*, 119, 1239
- Sneden, C. 1973, *ApJ*, 184, 839
- Sneden, C., Gratton, R.G., & Crocker, D.A. 1991, *A&A*, 246, 354 (GS)
- Sneden, C., Kraft, R.P., Prosser, C.F., & Langer, G.E. 1991, *AJ*, 102, 2001
- Sneden, C., McWilliam, A., Preston, G.W., Cowan, J.J., Burris, D.L., & Armosky, B.J., 1996, *ApJ*, 467, 819
- Sneden, C., Kraft, R.P., Shetrone, M.D., Smith, G.H., Langer, G.E., & Prosser, C.F. 1997, *AJ*, 114, 1964
- Sneden, C., Cowan, J.J., Evans, I.I., Fuller, G.M., Burles, S., Beers, T.C., & Lawler, J.E. 2000, *ApJ*, 533, 139
- Stephens, A. 1999, *AJ*, 117, 1771 (S99)
- Stetson, P.B. 1979, *AJ*, 84, 1149
- Stetson, P.B. 1984, *PASP*, 96, 128
- Suntzeff, N.B., Kraft, R.P., & Kinman, T.D. 1988, *AJ*, 95, 91
- Suntzeff, N.B., & Smith, V.V. 1991, *ApJ*, 381, 160
- Suntzeff, N.B., Mateo, M., Terndrup, D.M., Olszewski, E.W., Geisler, D., & Weller, W. 1993, *ApJ*, 418, 208
- Talbot, R.J., & Arnett, W.D. 1971, *ApJ*, 170, 409
- Tsujimoto, T., Nomoto, K., Yoshii, Y., Hashimoto, M., Yanagida, S., & Thielemann, F.-K. 1995, *MNRAS*, 277, 945
- Tyson, N.D. 1988, *ApJ*, 329, L57
- Unavane, M., Wyse, R.F.G., & Gilmore, G. 1996, *MNRAS*, 278, 727
- van Agt, S.L.Th.J. 1967, *Bull. Astron. Inst. Netherlands*, 19, 275
- Vladilo, G. 1998, *ApJ*, 493, 583 (V98)
- Wassermann, G.J., Busso, M., & Gallino, R. 1996, *ApJ*, 466, 109
- Vogt, S.S., et al. 1994, *SPIE*, 2198, 362
- Westin, J., Sneden, C., Gustafsson, B., & Cowan, J. J. 2000, *ApJ*, 530, 783
- Wolfe, A.M., Lanzetta, K.M., Foltz, C.B., & Chaffee, F.H. 1995, *ApJ*, 454, 698
- Yanny, B., et al. 2000, *AJ*, in press (astro-ph/0004128)

York, D.G., Dopita, M., Green, R., & Bechtold, J. 1986, ApJ, 311,  
610  
Zinn, R. 1978, ApJ, 225, 790

Zinn, R. 1993, in The Globular Cluster-Galaxy Connection, ASP  
Conference Series, Vol. 48, edited by G. Smith and J. Brodie (San  
Francisco: ASP), 603



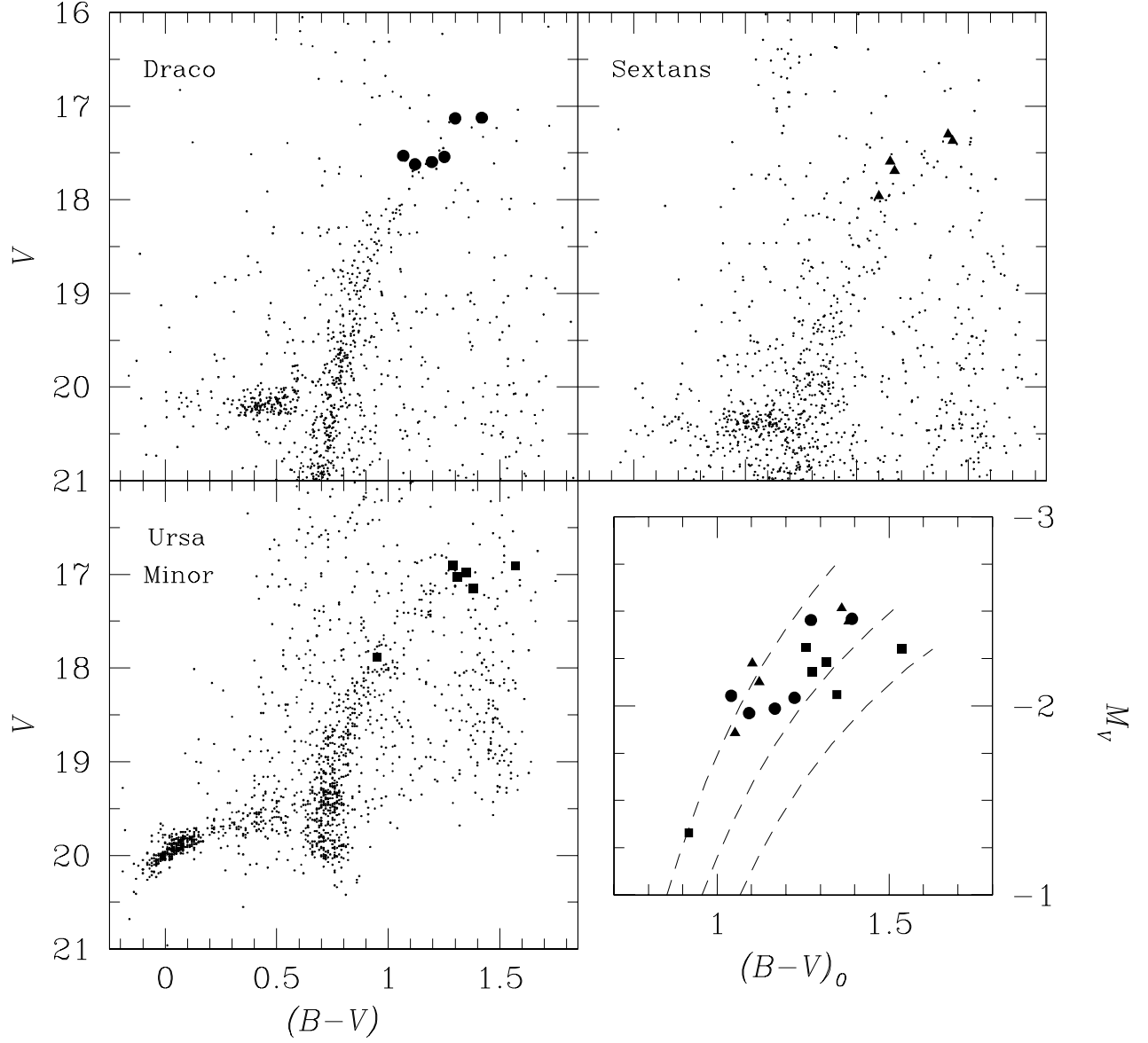


FIG. 1.—  $BV$  color magnitude diagrams for the three dSph galaxies in our program: Draco, Sextans and Ursa Minor. The red giant branch stars for which we have HIRES spectra are indicated by the circles (Draco), triangles (Sextans), and squares (Ursa Minor). The four Draco stars observed by Shetrone et al. (1998) are also shown in the first panel. Photometric data for Draco, Sextans and Ursa Minor are from Stetson (2000), Suntzeff et al. (1993) and Cudworth et al. (2000), respectively. The lower right panel shows the location of our program stars in the  $M_V$ - $(B-V)_0$  plane. Dashed lines show 13 Gyr isochrones from Bergbusch & Vandenberg (1992) having metallicities of  $[\text{Fe}/\text{H}] = -2.26, -1.66$  and  $-1.26$  dex. The symbol are the same as in the proceeding panels.

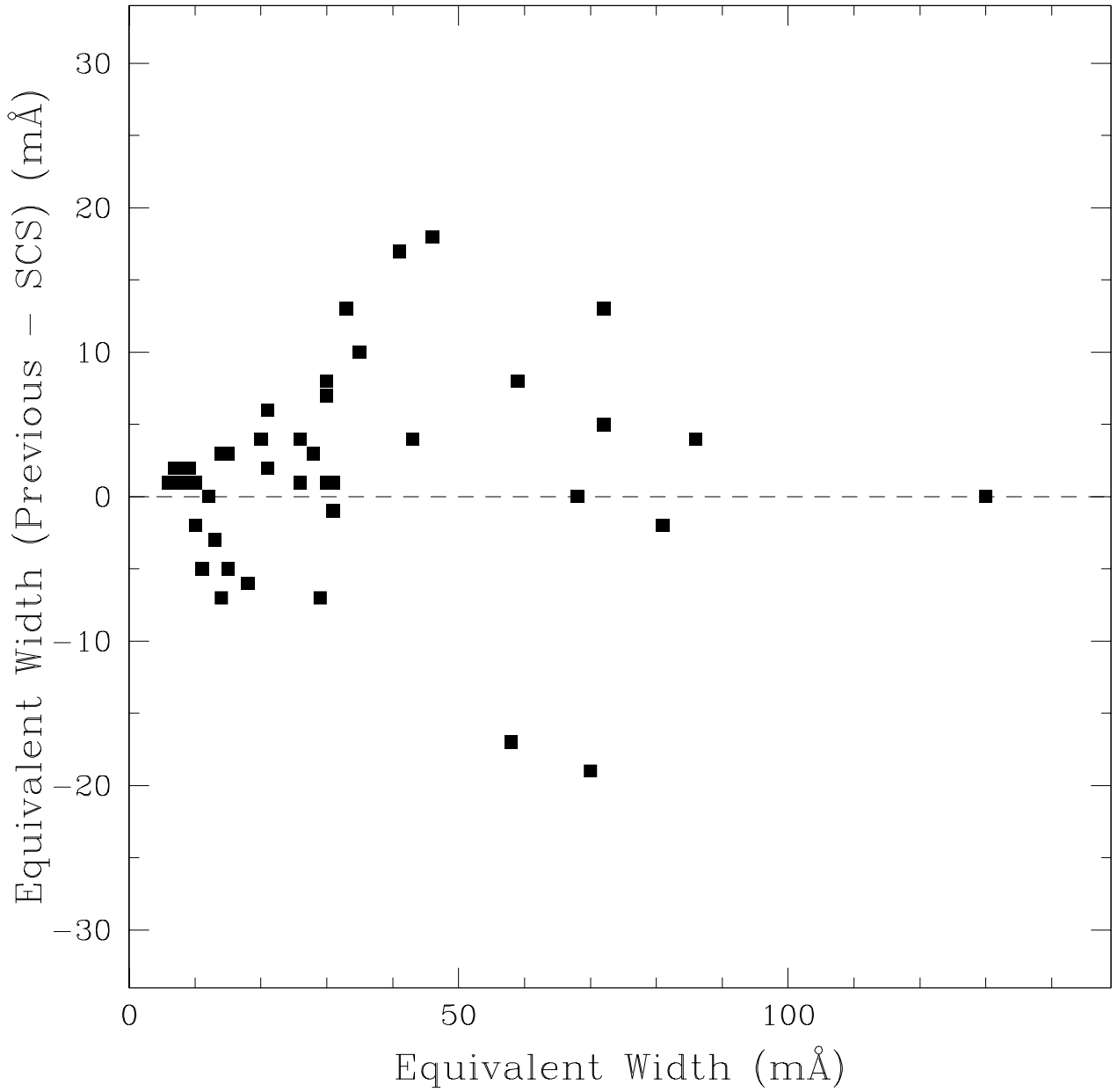


FIG. 2.— Comparison of equivalent widths for the globular cluster red giants presented in Table 3 with those previously reported by Sneden et al. (1991) and Kraft et al. (1992).

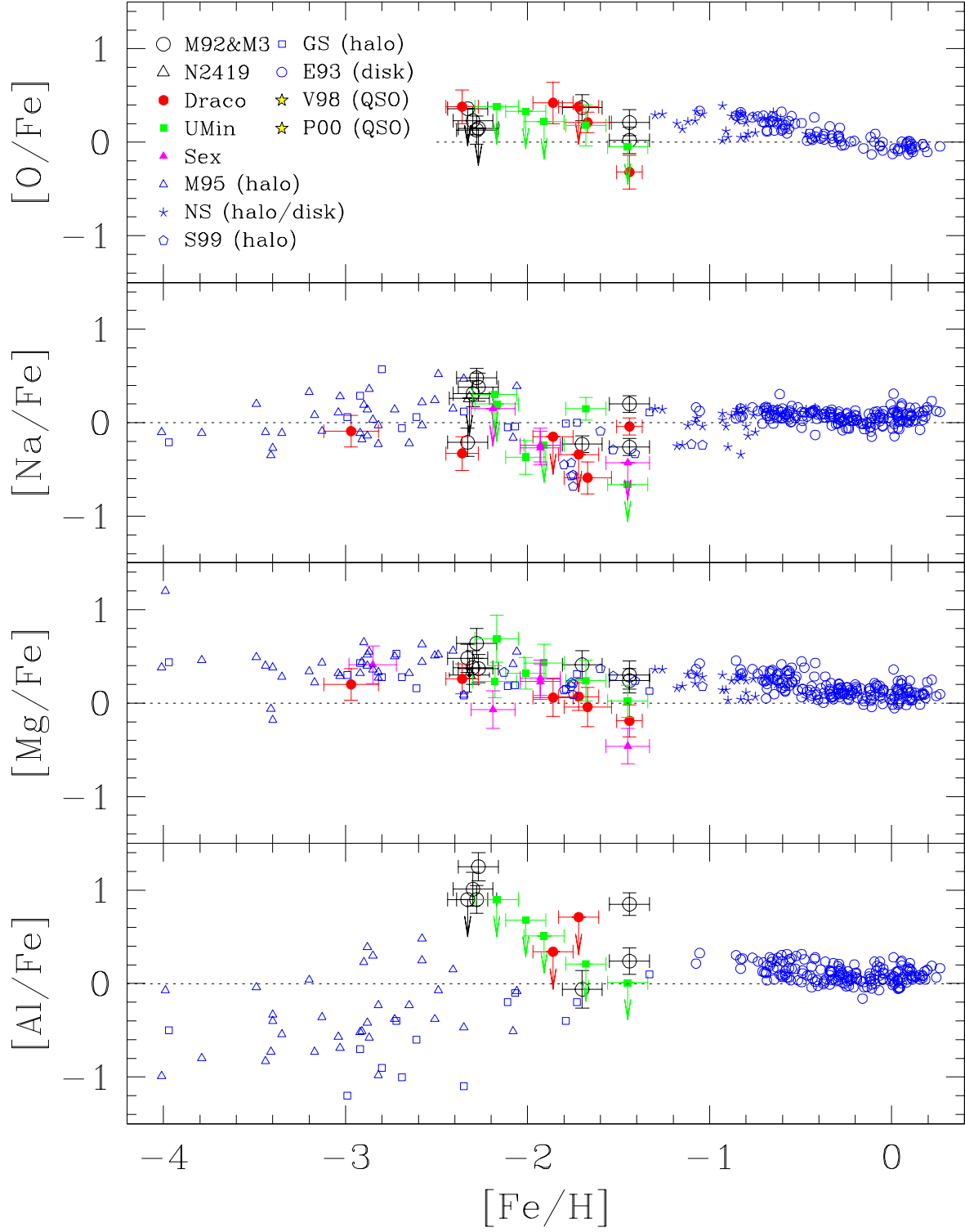


FIG. 3.— Abundance ratios for light (Na, Al) and alpha (O, Mg) elements, plotted against logarithmic iron-to-hydrogen ratio,  $[\text{Fe}/\text{H}]$ . The dashed line shows the solar ratios. The key to the symbols is given in the upper panel. The halo field star samples are from McWilliam et al. (1995; M95), Nissen & Schuster (1997; NS), Stephens (1999; S99), and the series of papers by Gratton (1989), Sneden et al. (1991) and Gratton & Sneden (1988; 1991; 1994; GS). Disk stars are from Edvardsson et al. (1993; E93) and Nissen & Schuster (1997; NS). Element abundances for damped Ly $\alpha$  absorbers in the direction of several QSOs are taken from Vladilo (1998; V98) and Pettini et al. (2000; P00).

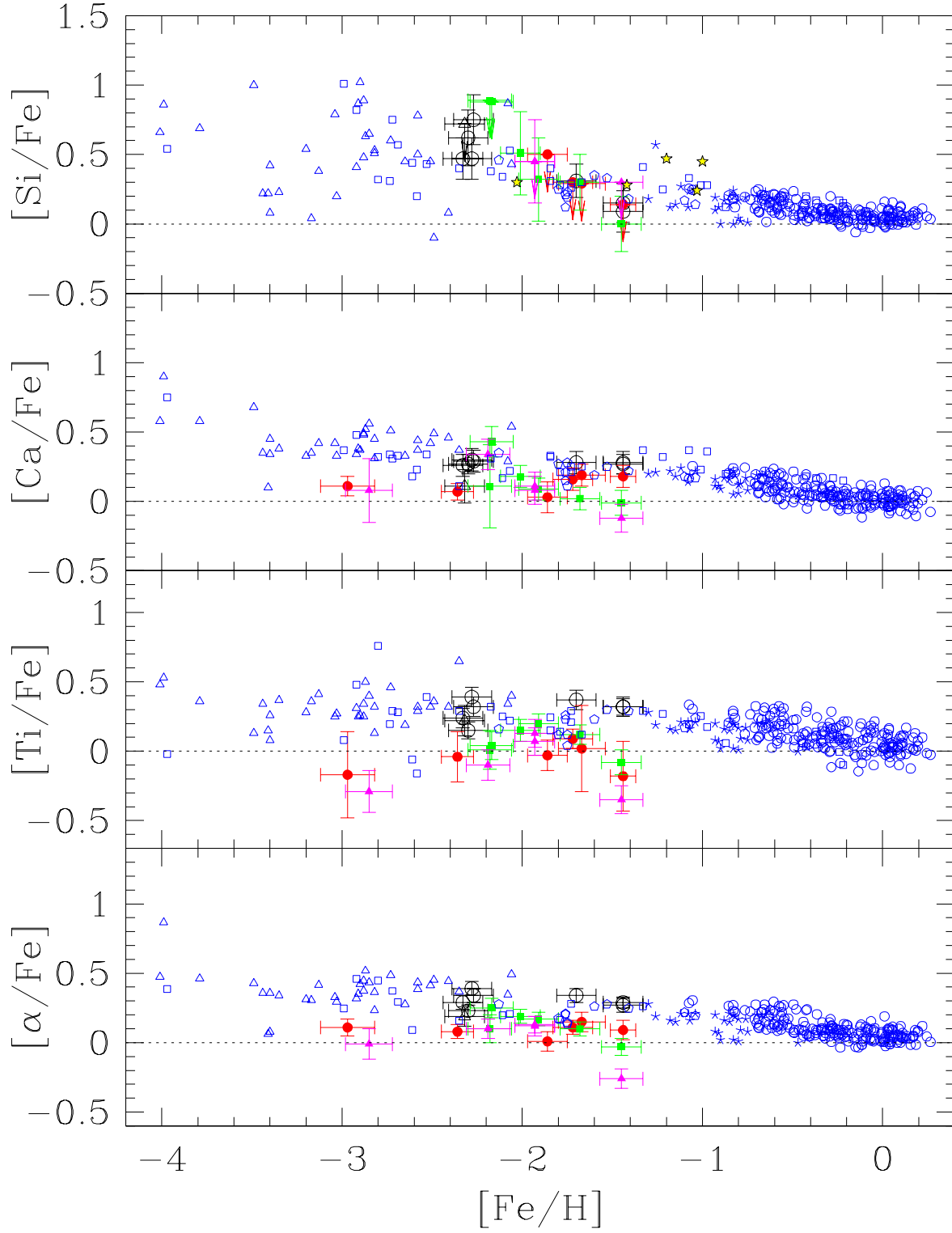


FIG. 4.— Abundance ratios for additional alpha elements (Si, Ca, Ti) plotted against  $[\text{Fe}/\text{H}]$ . The lower panel shows the *mean* alpha element abundance ratio, taken here as  $[\alpha/\text{Fe}] = \frac{1}{3}([\text{Mg}/\text{Fe}] + [\text{Ca}/\text{Fe}] + [\text{Ti}/\text{Fe}])$ . The symbols are the same as in Figure 3.

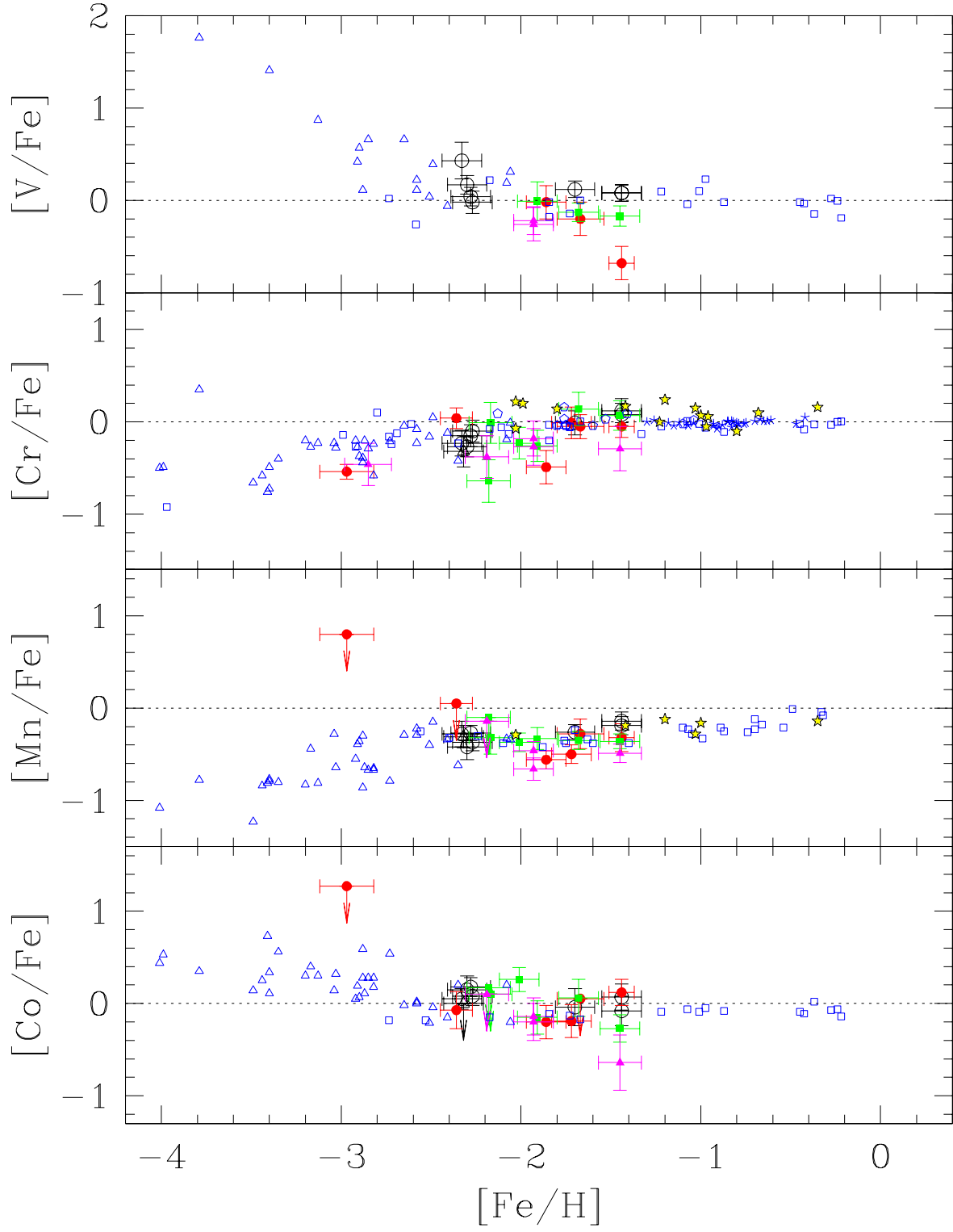


FIG. 5.— Abundance ratios for iron peak elements (V, Cr, Mn, Co) plotted against  $[\text{Fe}/\text{H}]$ . The symbols are the same as in Figure 3.

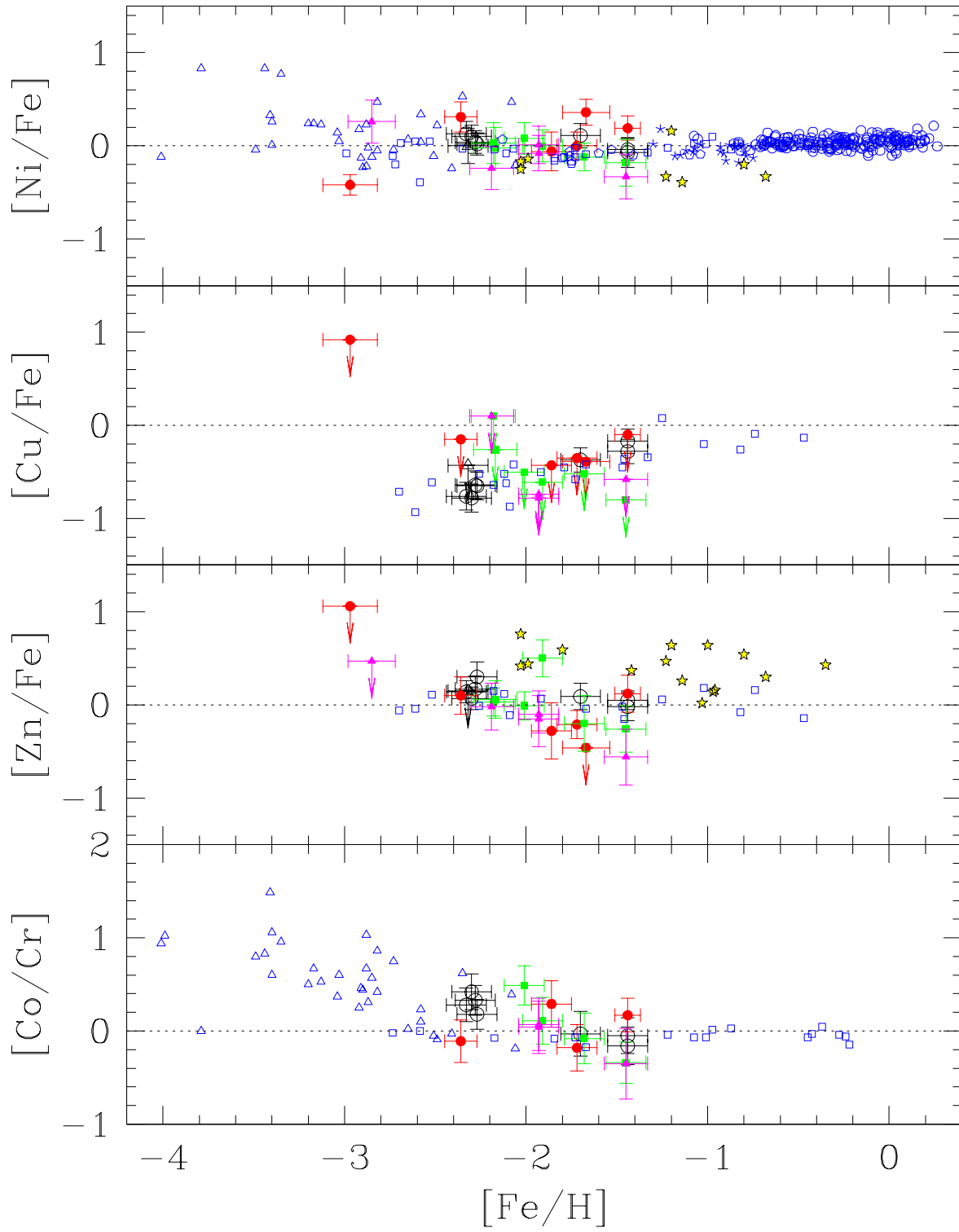


FIG. 6.— Abundance ratios for additional iron peak elements (Ni, Cu, Zn) plotted against  $[\text{Fe}/\text{H}]$ . The lower panel shows the dependence of  $[\text{Co}/\text{Cr}]$  on metallicity. The symbols are the same as in Figure 3.

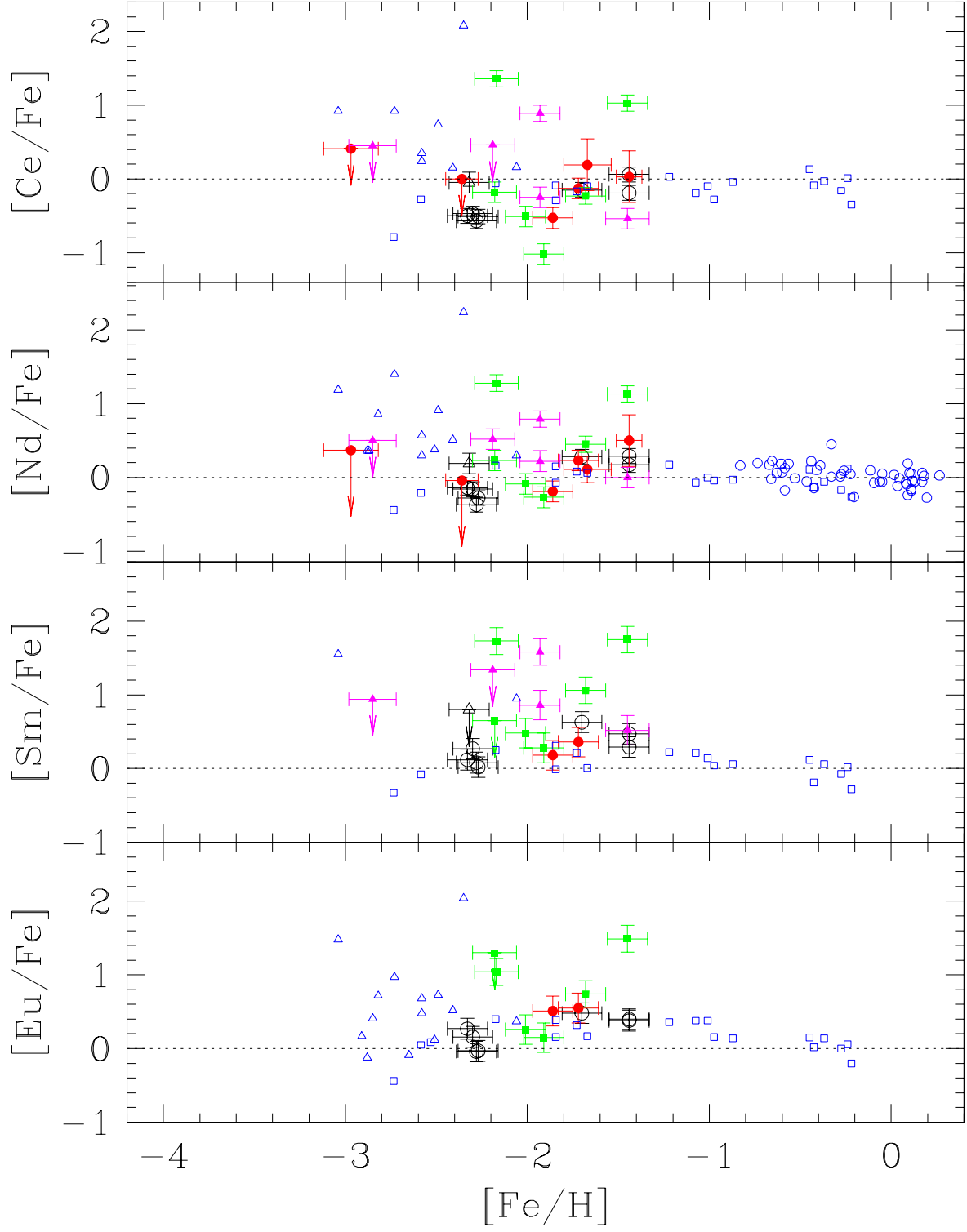


FIG. 7.— Abundance ratios for heavy elements (Ce, Nd, Sm, Eu) plotted against  $[Fe/H]$ . The symbols are the same as in Figure 3.

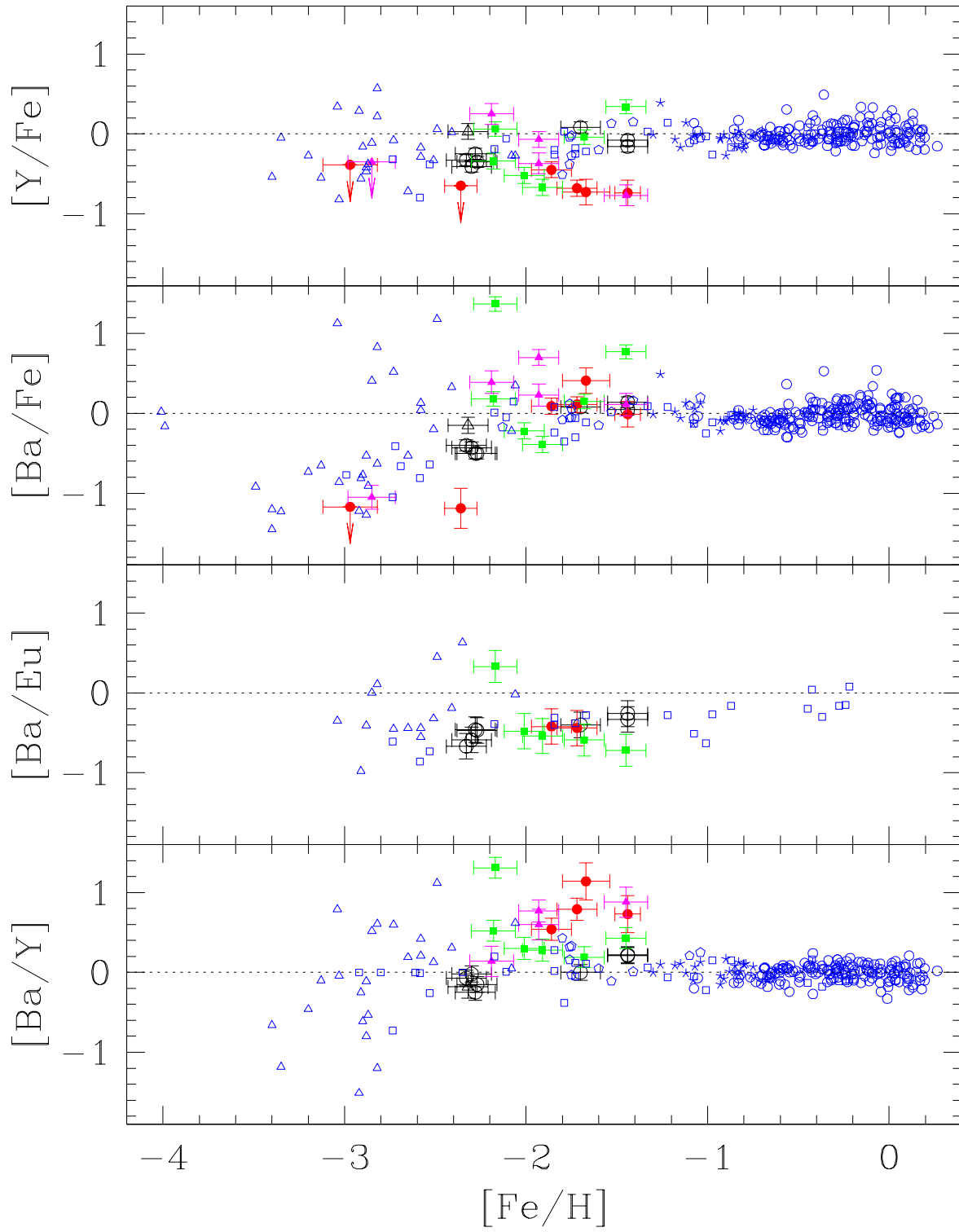


FIG. 8.— Abundance ratios for neutron-capture elements (Y, Ba) are plotted against  $[\text{Fe}/\text{H}]$  in the upper two panels. The lower two panels show the dependence of  $[\text{Ba}/\text{Eu}]$  and  $[\text{Ba}/\text{Y}]$  on metallicity. The symbols are the same as in Figure 3.